PLOS GENETICS

RESEARCH ARTICLE

# Behavioral screening reveals a conserved residue in Y-Box RNA-binding protein required for associative learning and memory in *C. elegans*

**Ashley N. Hayden[1,2], Katie L. Brandel[1,2], Edward W. Pietryk[2,3], Paul R. Merlau[2], Priyadharshini Vijayakumar[2], Emily J. Leptich[1,2], Elizabeth S. Gaytan[2,4], Meredith I. Williams[2], Connie W. Ni[2,5], Hsiao-Tuan Chao[1,3,6,7,8], Jill A. Rosenfeld[3,9], Rachel N. Arey[2,10]***

**1** Department of Neuroscience, Baylor College of Medicine, Houston, Texas, United States of America, **2** Center for Precision Environmental Health, Baylor College of Medicine, Houston, Texas, United States of America, **3** Department of Molecular and Human Genetics, Baylor College of Medicine, Houston, Texas, United States of America, **4** Postbaccalaureate Research Education Program, Baylor College of Medicine, Houston, Texas, United States of America, **5** Department of Neuroscience, Rice University, Houston, Texas, United States of America, **6** Department of Pediatrics, Division of Neurology and Developmental Neuroscience, Baylor College of Medicine, Houston, Texas, United States of America, **7** Cain Pediatric Neurology Research Foundation Laboratories, Jan and Dan Duncan Neurological Research Institute, Texas Children's Hospital, Houston, Texas, United States of America, **8** McNair Medical Institute, The Robert and Janice McNair Foundation, Houston, Texas, United States of America, **9** Baylor Genetics Laboratories, Houston, Texas, United States of America, **10** Department of Molecular and Cellular Biology, Baylor College of Medicine, Houston, Texas, United States of America

* rachel.arey@bcm.edu





**Citation:** Hayden AN, Brandel KL, Pietryk EW, Merlau PR, Vijayakumar P, Leptich EJ, et al. (2024) Behavioral screening reveals a conserved residue in Y-Box RNA-binding protein required for associative learning and memory in *C. elegans*. PLoS Genet 20(10): e1011443. https://doi.org/10.1371/journal.pgen.1011443

**Editor:** Pablo Wappner, Instituto Leloir, ARGENTINA

**Received:** May 17, 2024

**Accepted:** September 30, 2024

**Published:** October 18, 2024



**Data Availability Statement:** All relevant data are within the manuscript and its Supporting Information files.

**Funding:** This work was supported by a NIH Director's New Innovator Award (DP2NS132372), support from the Whitehall Foundation (https://www.whitehall.org/), and Glenn Foundation for Medical Research and AFAR Grant for Junior Faculty (https://www.afar.org/) to RNA. ANH is supported by and F31 NRSA F31NS129312-01 and

## Abstract

RNA-binding proteins (RBPs) regulate translation and plasticity which are required for memory. RBP dysfunction has been linked to a range of neurological disorders where cognitive impairments are a key symptom. However, of the 2,000 RBPs in the human genome, many are uncharacterized with regards to neurological phenotypes. To address this, we used the model organism *C. elegans* to assess the role of 20 conserved RBPs in memory. We identified eight previously uncharacterized memory regulators, three of which are in the *C. elegans* Y-Box (CEY) RBP family. Of these, we determined that *cey-1* is the closest ortholog to the mammalian Y-Box (YBX) RBPs. We found that CEY-1 is both necessary in the nervous system for memory ability and sufficient to promote memory. Leveraging human datasets, we found both copy number variation losses and single nucleotide variants in *YBX1* and *YBX3* in individuals with neurological symptoms. We identified one predicted deleterious *YBX3* variant of unknown significance, p.Asn127Tyr, in two individuals with neurological symptoms. Introducing this variant into endogenous *cey-1* locus caused memory deficits in the worm. We further generated two humanized worm lines expressing human *YBX3* or *YBX1* at the *cey-1* locus to test evolutionary conservation of *YBXs* in memory and the potential functional significance of the p.Asn127Tyr variant. Both *YBX1/3* can functionally replace *cey-1*, and introduction of p.Asn127Tyr into the humanized *YBX3* locus caused memory

Baylor Research Advocates for Student Scientists https://give.bcm.edu/get-involved/brass/). HTC's research effort is partially supported by The Robert and Janice McNair Foundation (https://mcnairfoundation.org/), Burroughs Wellcome Fund (https://www.bwfund.org/), Cain Pediatric Neurology Research Foundation Laboratories (https://www.bcm.edu/departments/pediatrics/research/cain-foundation-laboratories), Anne and Bob Graham, and the Child Neurology Foundation and Society. (https://www.childneurologyfoundation.org/about-cnf/). KBA is supported by a NSF GRFP (DGE-349937), EWP is supported by an NRSA (F31GM151846), EJL is funded by an NRSA (F31AG081095), and ESG is funded by BCM PREP (R25GM069234). The funders had no role in study design, data collection and analysis, decision to publish, or preparation of the manuscript.

**Competing interests:** The authors have declared that no competing interests exist.

deficits. Our study highlights the worm as a model to reveal memory regulators and identifies YBX dysfunction as a potential new source of rare neurological disease.

## Author summary

Memory relies on RNA translation, often controlled by RNA-binding proteins (RBPs). RBP dysfunction has been linked to memory issues in many neurological diseases. Here, we take advantage of the model organism *Caenorhabditis elegans* to determine the role of 20 RBPs in memory. We identify eight new memory regulators, including members of the CEY RBP family, which are closely related to the human YBX RBPs. We found that CEY-1 is required for memory in *C. elegans* and enhances memory when overexpressed. Taking advantage of human genome sequencing data, we found three individuals with the same genetic variant in *YBX3*, two of which have neurological symptoms including intellectual disability. Introducing this same variant into the CEY-1 protein caused memory deficits, suggesting the variant may cause dysfunction *in vivo*. To confirm this in the context of the mammalian genes, we made *C. elegans* that express the YBX3 variant protein instead of CEY-1 to model the functional consequences of the human *YBX3* variant. Again, we observed memory deficits. Our study shows the utility of *C. elegans* in discovering new memory-regulating RBPs and highlights a potentially conserved role for the CEY/YBX proteins in memory. Moreover, our findings suggest that dysfunction in the YBX RBPs may contribute to human neurological disease, beckoning future human and mammalian studies.

## Introduction

Careful regulation of RNA localization, translation, and stability is essential for the proper functioning of all tissues but is especially important in the nervous system. Neurons are composed of subcellular compartments, specifically somatic, axonal, and dendritic regions, each of which possesses a specialized and functionally distinct proteome. Moreover, these subcellular compartments must respond dynamically, and often uniquely, to external stimuli. A prominent example of this is local mRNA translation in response to plasticity-inducing stimuli, which is necessary for learning and memory [1,2]. In this instance, both the pre- and post-synaptic compartment can undergo local protein synthesis in response to the same plasticity-inducing stimulus [3,4], yet mRNAs translated in response to that stimulus are compartment-specific, likely due to distinct mRNA regulators.

RNA-binding proteins (RBPs) are involved in each step of RNA regulation in neurons, controlling target RNA splicing, polyadenylation, localization, translation, and stability [5]. As such, their proper function is essential for neuronal plasticity and its associated behaviors–especially learning and memory. The importance of understanding the role of RBPs in the nervous system is underscored by a growing body of evidence that their dysfunction results in neurological disease, including disorders ranging from neurodevelopmental disorders to neurodegenerative disease [6–8]. RBP-associated disorders often include symptoms of behavioral abnormalities and cognitive impairments, including Fragile X Messenger Ribonucleoprotein (*FMR1*) in Fragile X syndrome involving cognitive impairment, PUMILIO1 (*PUM1*) associated developmental disability, ataxia, and seizures (PADDAS), Quaking (*QKI*) in schizophrenia, and both Heterogeneous Ribonucleoprotein K (*HNRNPK*) in Au-Kline syndrome

and *SON* in Zhu-Tokita-Takenouchi-Kim (ZTTK) syndrome both involving intellectual disability [9–13]. In fact, RBPs outweigh all other protein types in their prevalence of predicted deleterious variation in Mendelian disorders, especially those that are diseases of the nervous system [7]. However, despite their importance, many RBPs are unexamined in the nervous system. Barriers remain to systematic characterization of RBPs, as such studies remain relatively slow in mammals and the human genome encodes nearly 2000 RBPs, which would require extensive time and effort to comprehensively study [14,15]. Moreover, studying the tissue-specific function of RBPs is even more difficult as it requires challenging and costly genetic approaches. However, these issues can be circumvented in simpler model organisms like the nematode worm *Caenorhabditis elegans* that allow for low-cost, rapid screening of molecules in a tissue-specific manner.

*C. elegans* have a rich history of use in high-throughput approaches and led to the discovery of many new regulators of neurological phenotypes, including molecularly conserved behaviors [16–18]. Indeed, the use of the worm resulted in the discovery of many conserved regulators of disease, including those involving cognitive deficits [19–24]. The *C. elegans* genome encodes almost 900 RBPs, over 80% of which have mammalian orthologs [25], and can be studied using thousands of publicly available mutants, including those that allow for neuron-specific RNAi for rapid tissue-specific genetic screening [26,27]. Importantly, *C. elegans* offers the advantage of using these genetic tools to investigate the role of RBPs in memory and cognition, as they form molecularly conserved associative memories, including short-term (STM), intermediate-term (ITM), and long-term memories (LTM) [20,28–32]. Given its wealth of molecular tools, ease of genetic screening, and molecularly conserved memory, *C. elegans* is an excellent model system to define the functions of neuronal RBPs in learning and memory *in vivo*.

Here, we have used the worm to perform a neuron-specific, targeted screen to discover conserved RBPs that regulate associative memory. Altogether, we find that 80% of 20 screened RBPs are memory regulators, eight of which are novel memory molecules. Importantly, our approach reveals a family of RBPs that are practically uncharacterized in their nervous system function and are essential for associative memory ability in the worm: the *C. elegans* Y-Box (CEY) RNA binding protein family.

Of this family, we determine that CEY-1 is most closely related to mammalian YBXs and requires further study to understand the potentially conserved role of YBXs in the nervous system. We found that CEY-1 acts specifically in the nervous system to promote memory. We discovered that large copy number losses including the genomic loci of *YBX* genes, as well as other known neurodevelopment disorder associated genes, may be associated with neurological symptoms such as intellectual disability. Furthermore, we similarly describe one rare heterozygous variant in the human *YBX3* gene identified in two unrelated individuals with neurological symptoms. Importantly, introduction of the conserved *YBX3* variant into either endogenous *cey-1* locus or animals where the *cey-1* locus has been humanized results in memory deficits in the worm, supporting the idea that the *YBX3* variant we identified may contribute to human disease.

Altogether, we uncovered new associative memory regulators in a targeted screen of 20 conserved neuronal RBPs. We describe in detail a novel associative memory regulator, CEY-1/YBX, and highlight *C. elegans* as a discovery organism for associative memory regulators and potential disease-causing RBPs.

## Results

### Targeted screen identifies novel RBPs that regulate learning and memory

The *C. elegans* genome encodes a total of 887 predicted RBPs. Of those, 60% are conserved with mammals [33,34]; thus, the worm is an excellent system to rapidly screen RBPs for

conserved roles in memory. We prioritized candidate RBPs based on the following criteria to increase the likelihood of identifying memory regulators: 1) nervous system expression based upon transcriptomic studies, 2) evolutionary conservation with mammals, and 3) detection in synaptic regions across species, as RBPs are known to regulate plasticity at the synapse. By cross-referencing adult-only, neuron-specific transcriptomic datasets [24,35] as well as orthology tools including Wormcat and OrthoList2 [36,37], we identified 550 neuronally expressed RBPs that are orthologs of known mammalian RBPs. After filtering this list based upon detection in *C. elegans* and mammalian synapses [35,38–42], 313 RBPs met screening criteria. Of those, we proceeded with the top 20 most synaptically-enriched RBPs based on our previous work identifying the adult *C. elegans* synaptic transcriptome [38,43] for behavioral study.

We assessed the roles of these 20 RBPs in memory by performing adult-only RNAi in neuronally RNAi-sensitized animals *(punc119*::*sid-1)* [27] and measuring the effects of knockdown on well-established assays of positive olfactory associative memory [29,30]. In these assays, animals are trained to form a positive association with the neutral odorant butanone and food, and by varying the number of food-butanone pairings can elicit short- and intermediate-term (STM and ITM) and long-term memories (LTM). The molecular requirements for these memories, including glutamate receptors (STM, ITM, LTM), calcium-dependent signaling cascades (STM, ITM, LTM), protein synthesis (ITM, forgetting, and LTM), and CREB-dependent transcription (LTM), are shared with mammals [20,28–30] and other *C. elegans* associative behavioral assays such as aversive olfactory learning and memory, memory for touch habituation, gustatory memory, imprinted olfactory memory, and aversive pathogen memories, to name a few [22,32,44–50].

In our screen, we assayed the following behaviors after positive olfactory training: learning (0 min after training), protein synthesis-independent STM (30 min after training), and translation-dependent ITM (1 hr after training) (**Fig 1A**) [29,30]. Effects of RBP knockdown on transcription and translation-dependent LTM were assessed in RNAi-sensitized animals with an additional *egl-30* gain of function mutation *(egl-30(js126)*, *punc119*::*sid-1))* that increases $G_{\alpha q}$ signaling and confers the ability to form a LTM that is molecularly identical to wild-type animals with only one round of training, making them amenable to high-throughput screening (**Fig 1B**) [51].

Of the 20 RBPs tested, 80% regulate at least one type of memory (**Fig 1C**). Two classes of proteins known to be required for memory across species had multiple members represented in our screen candidates: the Pumilio and FBF RBP family (*Pumilio1/2* orthologs *puf-3*, *puf-5*, *puf-7*, and *puf-8*) as well as four proteins involved in translation initiation (eIF4/2α orthologs *gcn-2*, *ife-1*, *ife-3*, and *drr-2*). Pumilios have been linked to both LTM and working memory in *Drosophila melanogaster* and mice [52,53], and we have previously described their importance in *C. elegans* memory [38,43]. Similarly, eukaryotic translation initiation machinery eIF4E and eIF2α are required for memory formation, STM, and LTM in mice [54,55]. However, to the best of our knowledge the requirement for this molecular machinery in olfactory associative memory was not previously demonstrated in the worm. Validating these two classes of known memory regulators strengthens the likelihood that novel molecules identified in our screen have a conserved function in higher organisms. Indeed, we found that 40% of memory regulating RBPs in our screen were not previously associated with memory phenotypes, and are therefore novel, bolded in **Fig 1C**. Importantly, there were no significant differences in naïve chemotaxis to a chemoattractive concentration (0.1%) of butanone (**S2 Fig**) for any RBP condition and additionally, no learning deficits were detected after knockdown of any RBP in our screen (**S1 Fig**). Together, these results suggest the deficits or enhancements we identified in our screen are specific to memory and are not due to broad behavioral or neurological disruption. For all behavior results plotted quantitatively, see **S3 Fig**, and for raw data for behavior timepoints where RNAi significantly altered memory, see **S4 Fig**.

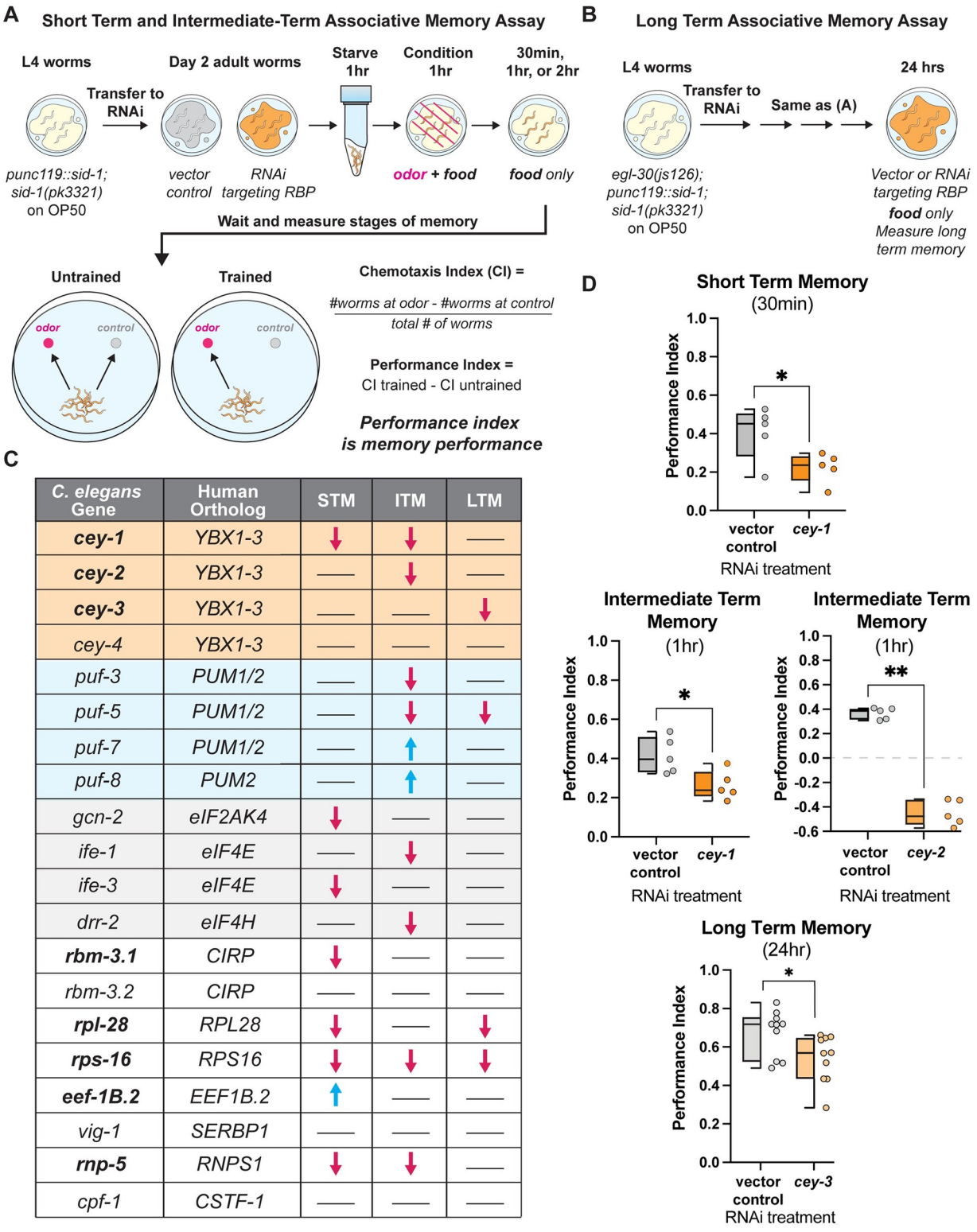


| *C. elegans* Gene | Human Ortholog | STM | ITM | LTM |
|---|---|---|---|---|
| ***cey-1*** | *YBX1-3* | ↓ | ↓ | — |
| ***cey-2*** | *YBX1-3* | — | ↓ | — |
| ***cey-3*** | *YBX1-3* | — | — | ↓ |
| *cey-4* | *YBX1-3* | — | — | — |
| *puf-3* | *PUM1/2* | — | ↓ | — |
| *puf-5* | *PUM1/2* | — | ↓ | ↓ |
| *puf-7* | *PUM1/2* | — | ↑ | — |
| *puf-8* | *PUM2* | — | ↑ | — |
| *gcn-2* | *eIF2AK4* | ↓ | — | — |
| *ife-1* | *eIF4E* | — | ↓ | — |
| *ife-3* | *eIF4E* | ↓ | — | — |
| *drr-2* | *eIF4H* | — | ↓ | — |
| ***rbm-3.1*** | *CIRP* | ↓ | — | — |
| *rbm-3.2* | *CIRP* | — | — | — |
| ***rpl-28*** | *RPL28* | ↓ | — | ↓ |
| ***rps-16*** | *RPS16* | ↓ | ↓ | ↓ |
| ***eef-1B.2*** | *EEF1B.2* | ↑ | — | — |
| *vig-1* | *SERBP1* | — | — | — |
| ***rnp-5*** | *RNPS1* | ↓ | ↓ | — |
| *cpf-1* | *CSTF-1* | — | — | — |

**Fig 1. Targeted screen of 20 conserved neuronal RBPs reveals eight novel associative memory regulators.** (**A**) Short-term and intermediate-term associative memory (STM and ITM) assay workflow using adult-only RNAi knockdown. Worms that are neuronally sensitive to RNAi, LC108*(usIS69[myo-2p::mCherry + unc119p::sid-1])*, were starved for 1 hour, conditioned for 1 hour, and tested immediately for 1x learning (0 min) via chemotaxis assays, or transferred onto holding plates with OP50 for 0.5, 1, or 2 hours after conditioning, then tested for STM and ITM changes. Memory performance is calculated by comparing the trained and untrained chemotaxis indices. (**B**) The long-term associative memory

(LTM) assay workflow is identical to that for STM/ITM except worms have an additional *egl-30(js126)* mutation that allows for LTM formation after just 1x training. Worms are tested immediately for 1x learning (0 min) via chemotaxis assays or transferred onto holding plates with RNAi for 16–24 hours after conditioning, then tested for LTM changes. (**C**) Results of our targeted screen of 20 RBPs reveals eight novel associative memory regulators. All RBPs screened are shown and include the *C. elegans* gene, its mammalian protein ortholog, and any STM, ITM, or LTM changes. Blue arrows indicate enhanced memory while pink arrows indicate decreased memory; lines indicate memory did not change. Novel memory regulators not reported in existing literature are bolded. For full screen results, see **S4 Fig**, and for significance quantification see **S3 Fig**. (**D**) Each member of the CEY RBP family plays a novel, unique role in memory. Adult-only RNAi knockdown of *cey-1* in neuronally-sensitized worms causes STM and ITM deficits, *cey-2* knockdown causes ITM deficits, and *cey-3* knockdown causes LTM deficits. Box and whisker plot: the center line denotes the median value (50th percentile) while the box contains the 25th to 75th percentiles. Whiskers mark the 5th and 95th percentiles. Mann-Whitney test comparing ranks. n = 10 per RNAi treatment. $^{*}p<0.05$, $^{**}p<0.01$.

https://doi.org/10.1371/journal.pgen.1011443.g001

## Identification of CEY family as novel memory regulators

Strikingly, all members of the *C. elegans* Y-Box (CEY) RBP family (*cey-1-4*), orthologs of the mammalian *Y-box binding* (*YBX*) family, met our screening criteria despite being uncharacterized in learning and memory behavior. The CEY RBPs regulate fertility in the worm [56,57], and mammalian YBX proteins are translational regulators involved in cancer metastasis and cell cycle progression [58–61]. Here we found that three of the four CEY proteins screened regulate memory, with each CEY involved in its own molecularly distinct form of memory (**Fig 1D**); *cey-1* is required for STM and ITM, *cey-2* is required for ITM, *cey-3* is required for LTM, and *cey-4* knockdown had no detectable effect on behavior. To our knowledge, this is the first documented behavioral phenotype regulated by CEY RBPs.

As there are no reported neuronal phenotypes associated with the CEY RBPs, we further examined their expression pattern based on previous transcriptomic profiling datasets. Single-cell RNA-seq data generated from neurons isolated from L4 larval animals revealed broad expression of *cey-1* and *cey-4*, while *cey-2* is only detected in eight neurons (**S5 Fig**) [62,63]. *cey-3* is not detected in any neurons at L4 but is detected in adult neuron-specific datasets [24,40], highlighting the importance of compiling multiple transcriptomic datasets to choose our screen candidates.

Similar to their *C. elegans* orthologs, the mammalian YBX proteins are relatively understudied with regards to behavioral phenotypes or their function in the adult nervous system, though YBX1 is reported to be involved in neural stem cell development [64]. Similar to *cey-1*, *YBX1* is broadly expressed throughout the nervous systems of humans, adult macaques, and rats [65]. In these mammals, *YBX1* is expressed in memory-regulating regions including the hippocampus, parahippocampal cortex, and dentate gyrus [65]. *YBX3* is also broadly expressed, including in memory-regulating regions, while *YBX2* is thought to be restricted to non-neuronal tissues [66,67]. Importantly, YBX1 is reported to bind to plasticity-associated mRNAs, including *GluR2* mRNA and *CaM1* mRNA, in an activity-dependent manner, making the YBXs promising candidates as novel essential memory molecules in mammals [68]. Moreover, both YBX1 and YBX3 proteins are detected in mouse hippocampal post-synaptic densities, suggesting that they have the potential to regulate local translation in a brain region critical for memory [69]. In non-neuronal tissues, CEYs and YBX proteins appear functionally conserved; both worm and mammalian proteins regulate polysome formation [56,70,71], suggesting that we can study conserved functions of this class of RBP in the worm.

To strengthen the translatability of our findings by focusing on conserved functions, we decided to study the *C. elegans* ortholog(s) that are the most closely related to the YBX proteins [60,61,64,72,73]. To this end, we performed phylogeny and homology analysis using MegaX and DIOPT [74,75] and found that *cey-1* is the primary *C. elegans YBX* ortholog, closer in similarity to the *YBXs* than other CEY family members (**Fig 2A and 2B**). For example, the linker regions (NC9 and CC13) and Cold-Shock Domain (CSD) of CEY-1 are extremely similar to those of the YBX proteins (approximately 97% similar) (**Fig 2C**) [76,77]. At both the N- and

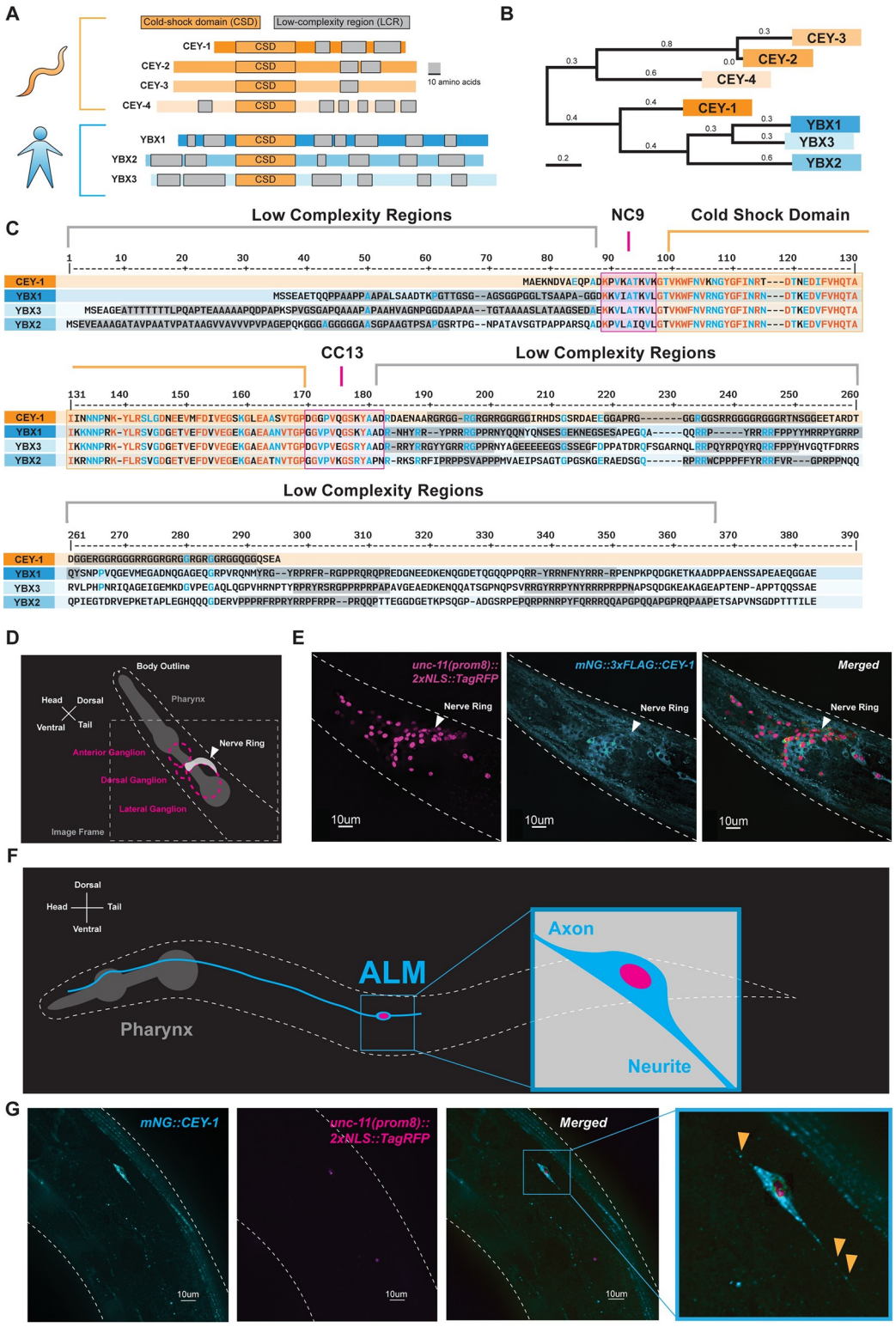


**Fig 2. CEY-1 is the closest ortholog to the human Y-box binding proteins.** (**A**) Diagram of the conserved protein domains of the *C. elegans* CEY RBPs and human YBX RBPs. *C. elegans* have four CEY RNA-binding proteins, CEY-1, CEY-2, CEY-3, and CEY-4, that are orthologs of the three mammalian Y-box binding proteins, YBX1, YBX2, and YBX3. All CEY/YBX RNA-binding proteins have a conserved cold-shock domain (CSD) that mediates RNA binding as well as one or more low complexity regions (LCRs) thought to be important for protein-protein interactions. Grey scale bar is 10

amino acids. (**B**) Phylogenetic tree generated using MegaX reveals that CEY-1 is more similar to the human YBX proteins than the other CEY RNA-binding proteins. (**C**) Protein sequence alignment of the CEY and human YBX binding proteins made with MultiAlin showing organization of protein domains. Highly conserved residues are depicted in red and blue. The cold-shock domains are highlighted in orange, the NC9 and CC13 linkers are highlighted in pink, and the low complexity regions are highlighted in grey. Domains were annotated according to SMART. (**D**) Diagram of microscopy images shown in (E). *C. elegans* head is labeled including the location of the pharynx and main neuronal ganglia/nerve rings. (**E**) CEY-1 is primarily localized to the cytoplasm at baseline conditions. Representative image of Day 2 adult worms with RFP-labeled neuronal nuclei *(unc-11(prom8)::2xNLS::TagRFP*) pseudocolored magenta and an endogenously mNeonGreen-tagged CEY-1 *(mNG::CEY-1)* pseudocolored cyan. (**F**) Diagram of microscopy images shown in (G). ALM sensory neuron has a stereotyped, easily identifiable anterior axonal projection and posterior neurite. (**G**) CEY-1 is localized to neurite and axon of the ALM sensory neuron at baseline conditions. Representative image of Day 2 adult worms with RFP-labeled neuronal nuclei *(unc-11(prom8)::2xNLS::TagRFP*) pseudocolored magenta and an endogenously mNeonGreen-tagged CEY-1 *(mNG::CEY-1)* pseudocolored cyan. Orange arrows indicate CEY-1 puncta.

https://doi.org/10.1371/journal.pgen.1011443.g002

C-termini, the CEY-1/YBX proteins are moderately conserved (approximately 60%). These are within low complexity regions, otherwise known as intrinsically disordered regions, responsible for protein-protein binding and stress granule formation [71,78].

Based on gene expression data, the expression pattern of *cey-1* and the mammalian YBX proteins is similarly broad across the nervous system [62,65–67,79–81]. Though previous studies using promoter-fusion approaches corroborate the transcriptomic evidence that *cey-1* is broadly expressed in the nervous system [56], we sought to verify that the protein is indeed expressed in neurons. We crossed the previously published *cey-1::GFP* promoter-reporter system [56] with a marker of neuronal nuclei (*unc-11(prom8)::2xNLS::TagRFP*) and validated their reported neuronal expression (**S6 Fig**). We confirmed these findings by verifying the neuronal localization of endogenous CEY-1 by crossing animals expressing an endogenously *mNeonGreen-tagged CEY-1 (mNG::CEY-1)* with *unc-11(prom8)::2xNLS::TagRFP* expressing animals (**Fig 2D and 2E**). We also examined if CEY-1 could potentially be localized to synaptic regions. As the protein is expressed in multiple neurons and tissues (**Fig 2D and 2E**) which interferes with visualization of specific synapses in the nerve ring, we examined if we could detect CEY-1 in the projections of the ALM neuron. The ALM neuron is isolated in the midbody and has an easily detectable and stereotyped anterior axonal projection and posterior neurite (**Fig 2F and 2G**). Though the posterior neurite of the ALM does not form any known synapses and may not behave in the same manner as a true dendrite [82,83], imaging the ALM would allow us to determine if CEY-1 was present in any neuronal projection. Endogenous CEY-1 was observed in both the neurite and axon of the ALM (**Fig 2G**), suggesting that this RBP could have the potential to localize to synaptic regions.

## CEY-1/YBX acts in neurons to regulate memory

To determine if *cey-1* acts in the nervous system to regulate learning and memory, we next tested if nervous-system specific *cey-1* knockdown causes memory deficits by performing adult-only, neuron-specific knockdown of *cey-1* using worms only expressing *sid-1* in the nervous system (*punc119::sid-1; sid-1(pk3321)*). Contrary to the mutants used in our initial screen, which can have off-target effects in other tissues, these worms lack *sid-1* in all tissues other than the nervous system, leading to RNAi specifically in the nervous system [27]. We confirmed that RNAi treatment in these animals resulted in reduced expression of CEY-1, by generating neuronally RNAi-sensitized *mNG::CEY-1* animals (**S7 Fig**). Our behavioral findings using this strain replicated the initial results of our screen: *cey-1* knockdown decreases both STM and ITM but not learning (**Fig 3A**). Importantly, we detected no motility or butanone chemotaxis deficits, although there are mild sensory deficits for isoamyl alcohol and nonanol (**S7 Fig**).

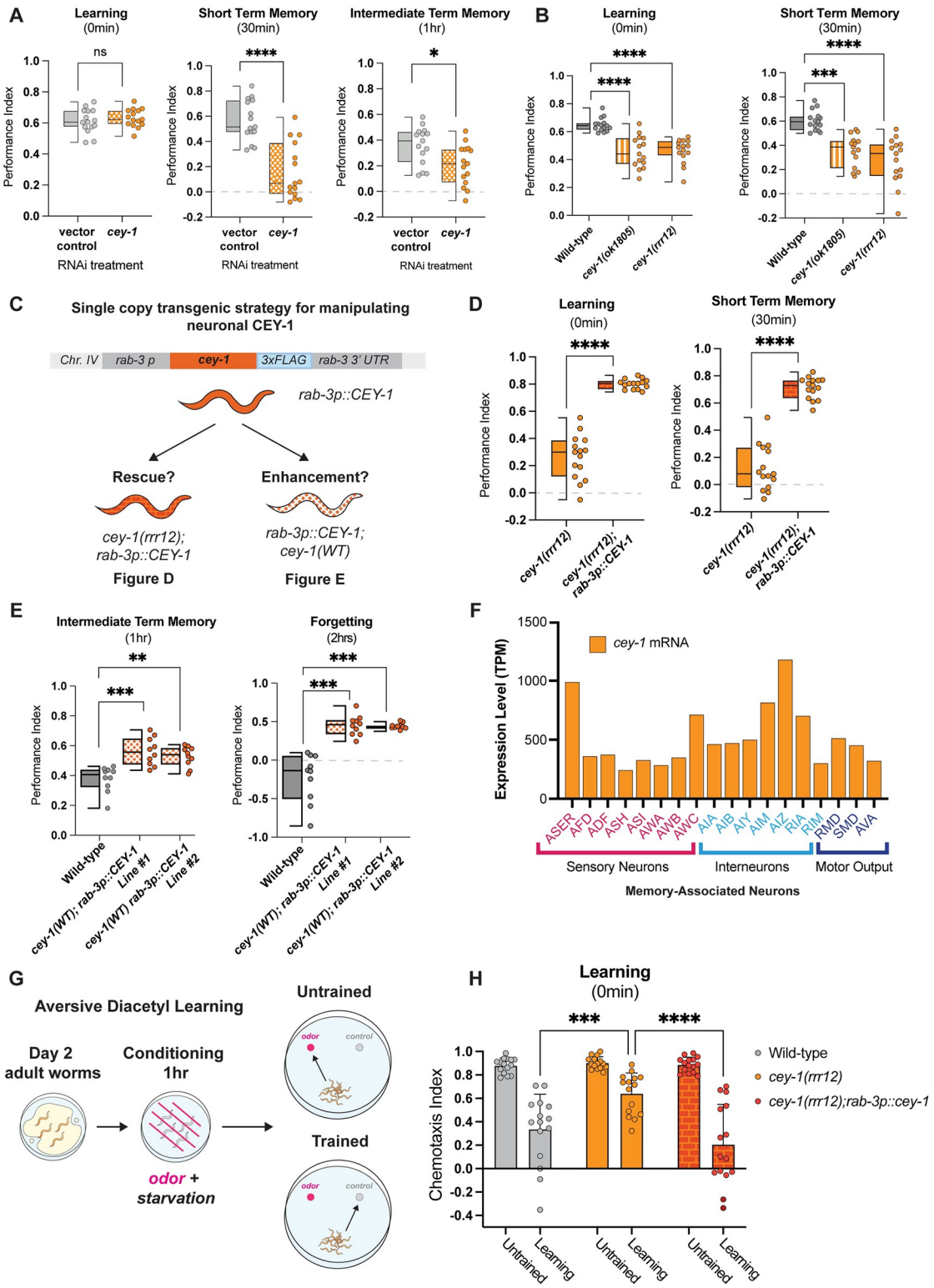


**Fig 3. CEY-1 promotes learning and memory in the *C. elegans* nervous system.** (**A**) Adult-only, neuron-specific knockdown of *cey-1* in *punc119*::*sid-1; sid-1(pk3321)* animals causes STM and ITM deficits. Box and whisker plot as in Fig 1. n = 15 per RNAi treatment. *p<0.05, ****p<0.0001. ns, not significant (p>0.05). (**B**) Loss-of-function mutants *cey-1(rrr12)* and *cey-1(ok1805)* have severe learning and memory deficits. Box and whisker plot as in Fig 1. n = 15 per genotype. ***p<0.001, ****p<0.0001. (**C**) Diagram of strategy to determine whether neuronal *cey-1* is sufficient to rescue and enhance memory. Worms that express a single

copy of *cey-1* only in the nervous system *(rab-3p*::*cey-1*::*rab-3 3'UTR; cey-1(rrr12))* were tested for phenotypic rescue in (D) while worms that have a single extra copy of *cey-1* only in the nervous system *(rab-3p*::*cey-1*::*rab-3 3'UTR; cey-1(+))* were tested in (E). (**D**) Single copy expression of *cey-1* in the nervous system *(rab-3p*::*cey-1*::*rab-3 3'UTR; cey-1(rrr12))* rescues loss-of-function learning and memory loss. Box and whisker plot as in Fig 1. n = 15 per genotype. ****p<0.0001. (**E**) Single copy overexpression of *cey-1* in the nervous system is sufficient to enhance memory *(rab-3p*::*cey-1*::*rab-3 3'UTR; cey-1(+))*. Box and whisker plot as in Fig 1. n = 15 per genotype. **p<0.01,***p<0.001. (**F**) Single-cell RNA-seq data from L4 hermaphrodites show that *cey-1* is expressed in every previously described memory-associated neuron, including those involved in aversive olfactory learning. (**G**) Workflow for aversive olfactory learning assays. Adult worms are starved for 1 hour in the presence of 100% diacetyl and tested immediately for 1x learning (0 min) via chemotaxis assays to 1% diacetyl. Learning performance is calculated by comparing the trained and untrained chemotaxis indices. (**H**) CEY-1 is required for learning in aversive paradigms, and behavioral defects in *cey-1(rrr12)* loss-of-function mutants are restored by nervous system-specific CEY-1 rescue. Box and whisker plot as in Fig 1. n = 15. ***p<0.001, ****p<0.0001.

https://doi.org/10.1371/journal.pgen.1011443.g003

However, given recent evidence that the *punc119*::*sid-1; sid-1(pk3321)* worms we used for may have leaky *cey-1* knockdown upon RNAi treatment in non-neuronal tissues such as the intestine [84], we pivoted to other genetic approaches to study *cey-1* in the nervous system. We examined the behavior of animals bearing two different loss-of-function *cey-1* alleles. Both animals exhibited severe deficits in learning and, as a result, inability to form a memory (**Fig 3B**). We ensured that both mutant alleles exhibited normal naïve chemotaxis to 10% butanone (**S8 Fig**), and further confirmed that the *cey-1(rrr12)* animals have no thrashing, motility, or butanone sensing deficits driving these results, as we used them for subsequent experiments (**S8 Fig**). Together, these results suggest the deficits we observed are learning and memory-specific and that *cey-1* is necessary for associative behaviors. We believe that by knocking down *cey-1* during adulthood (**Fig 3A**) we are circumventing loss of *cey-1* during neuronal development, which may be causing the more severe effects on learning seen in *cey-1* mutants (**Fig 3B**).

## Elevated neuronal CEY-1 is sufficient to enhance memory

We next asked if restoring *cey-1* function in nervous system was sufficient to rescue learning and memory deficits observed upon loss of *cey-1*. We generated *cey-1(rrr12)* loss of function animals that also express a single-copy knock-in transgene driving expression of *cey-1* specifically in the nervous system *(rab-3p*::*cey-1*::*rab-3 3'UTR; cey-1(rrr12))* (**Fig 3C**). We found that neuron-specific *cey-1* rescue is sufficient to restore the learning and memory deficits seen in *cey-1(rrr12)* mutants back to wild-type levels (**Figs 3D and S8**). Importantly, neither the *cey-1* loss of function mutants nor the neuronal *cey-1* rescue worms have deficits in butanone sensing, thrashing, or motility, suggesting that phenotypes recorded are memory-specific (**S8 Fig**).

Thus far, our data suggested that *cey-1* acts in the nervous system to promote memory. To test this hypothesis, we determined whether increasing *cey-1* expression in the nervous system would have beneficial effects on behavior. A single round of food-butanone training results in memory that persists for no longer than two hours in wild-type animals, and we asked if additional neuronal *cey-1* increased the duration of this memory, as has been observed with other memory promoting genetic manipulations [28,29,43]. Worms with (*rab-3p*::*cey-1*::*rab-3 3'UTR; cey-1(+))* showed enhanced memory (**Fig 3E**), as their memory persists longer than the average two hours, consistent with previous memory enhancers [28,29,43]. Collectively, our results show that *cey-1* is sufficient to increase memory when expressed only in the nervous system, suggesting that *cey-1* is a memory enhancer.

## CEY-1 is required for multiple associative behaviors

Despite its broad expression in the nervous system, we wanted to determine if *cey-1* was expressed in neurons involved in multiple types of learning and memory, and thus could be

required for other behaviors. Because the *C. elegans* nervous system is invariant [82,85], the identities of specific neurons involved in a variety of associative behaviors are known. Based upon previously generated L4 single-cell RNA-seq data, we find that *cey-1* is indeed detected in all canonical learning and memory-associated neurons, including those associated with gustatory plasticity, thermotaxis, and olfactory memory (**Fig 3F**) [51,86–92]. Therefore, we decided to test whether *cey-1(rrr12)* loss-of-function mutants also exhibit impaired learning in an aversive olfactory associative memory paradigm. In this assay, worms are starved in the presence of 100% diacetyl that is normally chemoattractive, forming a negative association (**Fig 3G**). Learning after aversive diacetyl conditioning requires neurons [32] distinct from those known to be involved in our appetitive memory paradigms [20,28,51]. We found that CEY-1 is also required for learning in this aversive paradigm, and the learning defects in *cey-1* loss-of-function mutants are restored by nervous system-specific CEY-1 rescue (**Fig 3H**). These results suggest that CEY-1 may be a broad regulator of the molecular mechanisms required for learning and memory across multiple neuronal circuits and paradigms.

## Copy number variant deletions in *YBX1* and *YBX3* may be associated with neurological symptoms, including intellectual disability

Human genomic datasets are increasingly linking RBP dysfunction to neurodevelopmental and neurological disorders, including those characterized by intellectual disability and cognitive dysfunction [6–8,93]. Therefore, we used copy number variation (CNV) datasets to determine if loss of the *YBXs* may potentially be associated with neurological dysfunction in humans. We used an open-access database, DECIPHER, that reports CNVs from 50,000 individuals [94]. We focused specifically on CNVs in *YBX1* and *YBX3*, as *YBX2* is not expressed in the adult human brain [65,67].

We found that many individuals with CNV deletions that include either *YBX1* or *YBX3*, as well as other genes have neurological symptoms (**Fig 4A**). The CNV deletions were variable in size, ranging from 1.59 Mb to 24.59 Mb. The most common symptom reported in individuals with CNV deletions including the *YBX*s is intellectual disability, as 37.5% of individuals with CNV deletions containing *YBX1* and 80% of individuals with CNV deletions in *YBX3* have intellectual disability (**Fig 4B**). Other common symptoms for individuals with *YBX1*-containing CNV deletions include epicanthus, microcephaly, and seizures, while individuals with *YBX3*-containing CNV deletions often exhibit strabismus and scoliosis. However, as is the case with the majority of CNVs, all *YBX*-containing CNV deletions included other genes that may be contributing to these individuals' phenotypes. In the case of *YBX1*, the minimal overlap between CNV losses affecting the *YBX1* loci is 1.08 Mb containing 34 genes, including two loci that are predicted to be loss of function intolerant: *Forkhead Box J3* (*FOXJ3*) [95] and *Solute Carrier Family 2 Member 1* (*SLC2A1*) [96]. *SLC2A1* is associated with autosomal dominant Dystonia 9 (MIM#601042) [96,97], GLUT1 deficiency syndrome 1 (MIM#606777) [98,99], GLUT1 deficiency syndrome 2 (MIM#612126) [100,101], Stomatin-deficient cryohydrocytosis with neurologic defects (MIM#608885) [102,103], and susceptibility to idiopathic generalized epilepsy 12 (MIM#614847) [104,105]. In the case of *YBX3*, the minimal overlap between CNV deletions affecting the *YBX3* loci is 3.24 Mb containing 68 genes, including three loci that are predicted to be loss of function intolerant: *ETS Variant Transcription Factor 6* (*ETV6*) [97], *Low Density Lipoprotein Receptor-related Protein 6* (*LRP6*) [98], and *Dual-Specificity Phosphatase 16* (*DUSP16*) [99]. However, unlike the loci surrounding *YBX1*, none of the loss of function intolerant loci around *YBX3* are known to cause monogenic neurological disease. Summary statistics for CNV DECIPHER data for *YBX1* can be found in **S9 Fig** and for *YBX3*

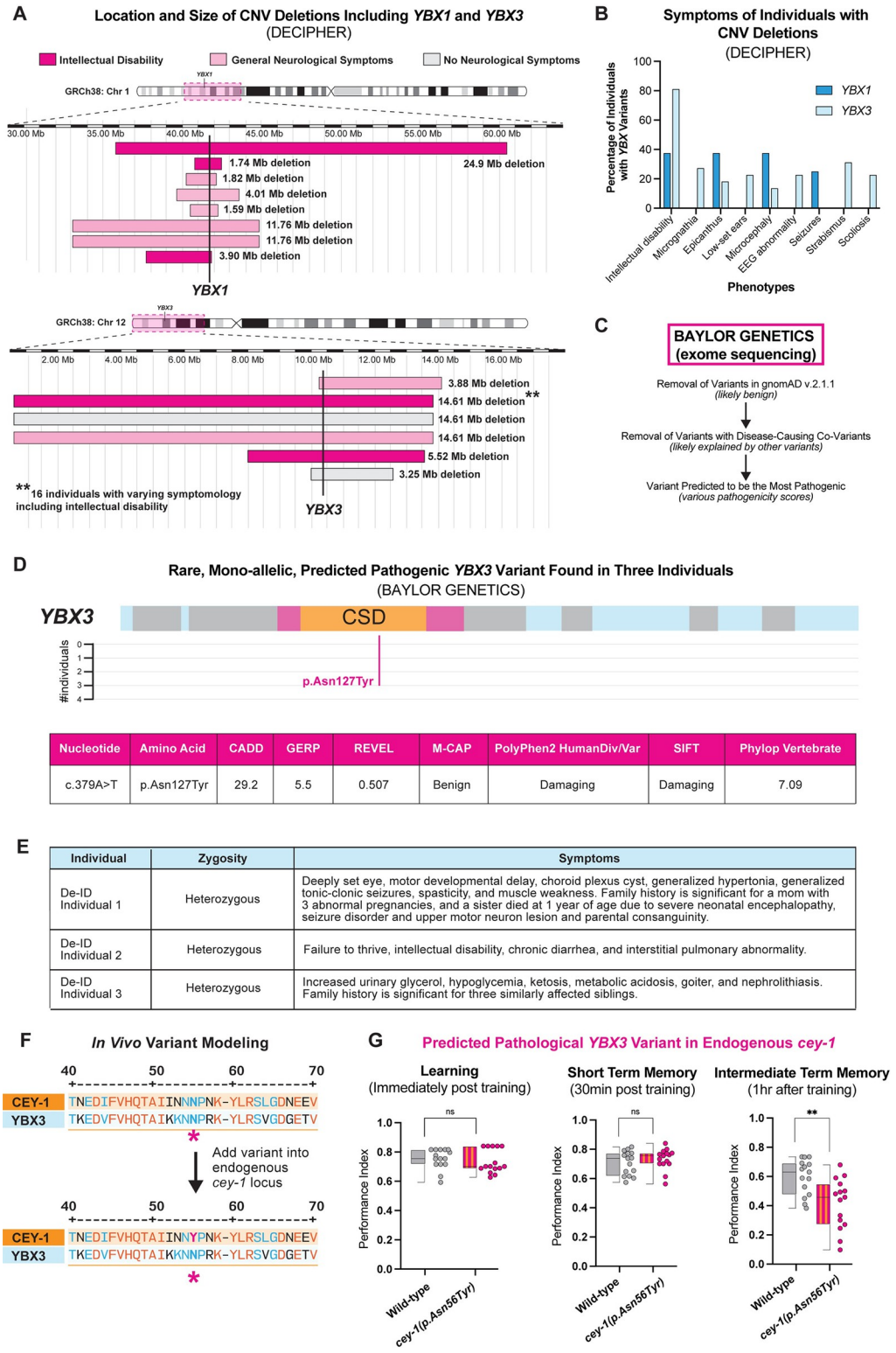


| Nucleotide | Amino Acid | CADD | GERP | REVEL | M-CAP | PolyPhen2 HumanDiv/Var | SIFT | Phylop Vertebrate |
|---|---|---|---|---|---|---|---|---|
| c.379A>T | p.Asn127Tyr | 29.2 | 5.5 | 0.507 | Benign | Damaging | Damaging | 7.09 |

E

| Individual | Zygosity | Symptoms |
|---|---|---|
| De-ID Individual 1 | Heterozygous | Deeply set eye, motor developmental delay, choroid plexus cyst, generalized hypertonia, generalized tonic-clonic seizures, spasticity, and muscle weakness. Family history is significant for a mom with 3 abnormal pregnancies, and a sister died at 1 year of age due to severe neonatal encephalopathy, seizure disorder and upper motor neuron lesion and parental consanguinity. |
| De-ID Individual 2 | Heterozygous | Failure to thrive, intellectual disability, chronic diarrhea, and interstitial pulmonary abnormality. |
| De-ID Individual 3 | Heterozygous | Increased urinary glycerol, hypoglycemia, ketosis, metabolic acidosis, goiter, and nephrolithiasis. Family history is significant for three similarly affected siblings. |

**Fig 4. Copy number variants in *YBX1* and *YBX3* found in individuals with neurological symptoms and *in vivo* modeling of a predicted pathogenic single nucleotide variant in YBX3.** (**A**) Location, size, and neurological symptoms associated with copy number variant (CNV) deletions reported in DECIPHER. The exact location of *YBX1* and *YBX3* are shown with a bold vertical line. The area around the gene affected by the CNV deletions is highlighted with a pink box on their respective chromosome ideograms at the top of the figure. CNVs where the individual had

neurological symptoms are in light pink, and CNVs where the individual had associated intellectual disability are in dark pink. (**B**) Intellectual disability is the most often associated symptom of patient CNV deletions containing the *YBX1* or *YBX3* loci based on DECIPHER. (**C**) Workflow to examine single nucleotide variants (SNVs) that may be disease-linked using the postnatal exome sequencing database from Baylor Genetics. Several strategies were used to remove likely non-pathogenic variants, including removing cases with known co-variants and removal of variants found in the general population (gnomAD v2.1.1). (**D**) Location and pathogenicity score of a rare heterozygous SNV in *YBX3* found in three de-identified individuals, two with indicated neurological symptoms. The variant we identified, p.Asn127Tyr, had the highest predicted pathogenicity using seven different metrics (see text). (**E**) Table of p.Asn127Tyr cases from Baylor Genetics de-identified exome sequencing dataset. Two of the three individuals have neurological symptomology reported, such as intellectual disability and seizures. (**F**) Location of p.Asn127Tyr variant shows conserved residues between CEY-1 and YBX3 and location of variant when introduced into the endogenous CEY-1 protein. (**G**) Introduction of p.Asn127Tyr into the endogenous *cey-1* locus (p.Asn56Tyr) causes ITM deficits. Box and whisker plot as in Fig 1. n = 15 per genotype. $^{**}p<0.01$, ns, not significant ($p>0.05$).

https://doi.org/10.1371/journal.pgen.1011443.g004

in **S10 Fig**. All individuals with CNV deletions in *YBX1* or *YBX3* as well as their DECIPHER phenotypic data can be found in **S1 Table.**

Taken together, these data suggest that loss of function CNVs including the *YBX1* and *YBX3* loci may be associated with neurological dysfunction; however, the confounding variable of multi-gene deletions prevents any direct association. As a result, we decided to model the rare *YBX3* c.379A>T (p.Asn127Tyr) variant for biological function *in vivo*.

## Introducing a predicted deleterious variant in *YBX3* into the endogenous *cey-1* locus causes memory deficits *in vivo*

The minimal overlap regions for CNV deletions containing *YBX1* and *YBX3* include loci beyond the gene of interest that are associated with monogenic neurological disorders and other diseases in humans. Therefore, single-nucleotide variants (SNVs) in the genes of interest may better link deleterious variants in single genes directly to neurological disorders [10,12,100–102] compared to CNVs with multi-gene deletions.

We received a deidentified dataset of *YBX* variants found through exome and genome sequencing completed at Baylor Genetics [103] to identify potentially deleterious SNVs in the *YBXs*. To determine variants of interest, we curated rare, heterozygous variants in postnatal individuals, as these are the most likely to be deleterious [104,105]. We first removed SNVs that were most likely not contributing to early developmental brain disorders by eliminating variants found in gnomAD v2.1.1 as well as cases where the subject's symptomology was explained by other variants in the genome (**Fig 4C**). We then used seven different pathogenicity metrics to determine which variants were the most likely to be deleterious, including CADD [106,107], GERP [108], REVEL [109], M-CAP [110], PolyPhen 2 [111], SIFT [112], and Phylop Vertebrate [113]. The variant with the highest overall pathogenicity scores was in *YBX3*: c.379A>T resulting in the amino acid change p.Asn127Tyr. The affected amino acid is in the Cold-Shock Domain of the YBX3 protein and, significantly, this variant is not reported in gnomAD v.2.1.1 nor gnomAD v4, suggesting it is rare (**Fig 4D**). We found this variant in three different individuals, two of which present with neurological symptoms such as intellectual disability and seizures (**Fig 4E**).

The p.Asn127 residue is highly conserved across species, including between *C. elegans* CEY-1 and human YBX3 (**Fig 4F**). Therefore, we decided to test the potential significance of this variant *in vivo* in *C. elegans* by introducing it into the endogenous *cey-1* locus and examining its effect on memory. We used CRISPR to introduce the same mutation into the endogenous *cey-1* gene at the same conserved residue as in YBX3: p.Asn56Tyr (*cey-1 p.Asn56Tyr*). We then tested for memory deficits at learning, STM, and ITM. Remarkably, introduction of the p.Asn56Tyr variant into *cey-1* caused ITM deficits, suggesting the variant may have

consequences on human neurological function (Fig 4G). Importantly, CEY-1 p.Asn56Tyr worms had no butanone sensing deficits or motility impairments (S11 Fig), suggesting that in this case, neurological dysfunction is memory-specific. We performed qRT-PCR and verified that while the *cey-1(rrr12)* allele is a true knockout that undergoes nonsense mediated decay [56], our p.Asn56Tyr variant has no significant effect on levels of *cey-1* mRNA, suggesting this SNV affects protein function rather than gene expression levels (S11 Fig). By using the worm to model one predicted damaging variant in *YBX3*, our findings suggest that *YBX3* may be of interest for human disease associations. Therefore, we decided to take our rare variant modeling a step further by using humanized worm strains expressing *YBX1/3*.

## *YBX1* and *YBX3* functionally replace *cey-1* in a humanized model and introduction of a predicated deleterious variant into *YBX3* causes memory deficits *in vivo*

Recent studies have highlighted the utility of humanized worm lines in phenotypic modeling of rare human gene variants *in vivo* [114–117]. We decided to use this CRISPR-based approach to determine whether the predicted damaging variant YBX3 p.Asn127Tyr, which we found in *YBX3* in two human individuals with neurological symptoms and one individual without neurological symptoms, affects YBX3 function in the context of memory. We created two humanized worm lines expressing either human *YBX1* or *YBX3* at the endogenous *cey-1* locus, thereby replacing *cey-1* (Fig 5A). These human genes are expressed similarly to endogenous *cey-1* at the mRNA level, as measured by qPCR (S12 Fig). In both cases, the human orthologs were able to functionally replace *cey-1*: learning, STM, and ITM were comparable to that of wild-type animals (**Figs 5B, 5C and S12**). Intriguingly, worms expressing *YBX3* displayed behavior that was nearly indistinguishable from wild-type animals, exhibiting normal forgetting at two hours post-training, while worms expressing *YBX1* still maintained a modest memory two hours post-training, suggesting potential differences in regulation during active forgetting (S12 Fig). Given *YBX3* functionally replaces *cey-1* in memory, we introduced the rare predicted deleterious variant p.Asn127Tyr into the humanized *YBX3* locus to determine if the variant would affect memory. Like when we mutated the endogenous *cey-1* gene (S11 Fig), this variant had no significant effect on *YBX3* mRNA levels (S12 Fig). When we examined their behavior, worms expressing *YBX3(p.Asn127Tyr)* have severe intermediate term memory deficits (Fig 5D), mirroring our findings with the equivalent variant inserted into the endogenous *cey-1* locus (Fig 4G). None of the humanized strains had impaired butanone sensing or motility, suggesting these deficits are memory-specific (S12 Fig). Taken together, our findings suggest a high degree of functional conservation between *cey-1* and *YBX3*.

We next attempted to determine the effect of the p.Asn127Tyr mutation on YBX3 function. Based upon Alphafold2 [118] predictions, the Asn127 residue is part of a long, disordered loop that connects two β-sheets of the YBX3 cold shock domain (S13 Fig). Since this residue is not buried within the organized part of the protein, it is not obvious how this mutation could affect protein structure. We turned to two prediction models, AlphaMissense [119] and Functional Characterization via Evolutionary Scale Models (FunC-ESMs, [120]), that predict the effect of mutations on protein function. Both models predicted that p.Asn127Tyr would be detrimental to protein function, with an AlphaMissense score of 0.998 on a scale of 0.0–1.0, which is 'likely pathogenic', and FunC-ESMs predicting a 'Total Loss'. Together, these prediction tools suggest that this residue is important for function.

Because the prediction models suggest that *YBX3(p.Asn127Tyr)* may produce a protein with reduced function, we tested whether or not we could rescue the behavioral phenotypes of worms expressing *YBX3(p.Asn127Tyr)* with a wild-type copy of CEY-1. We generated *YBX3*

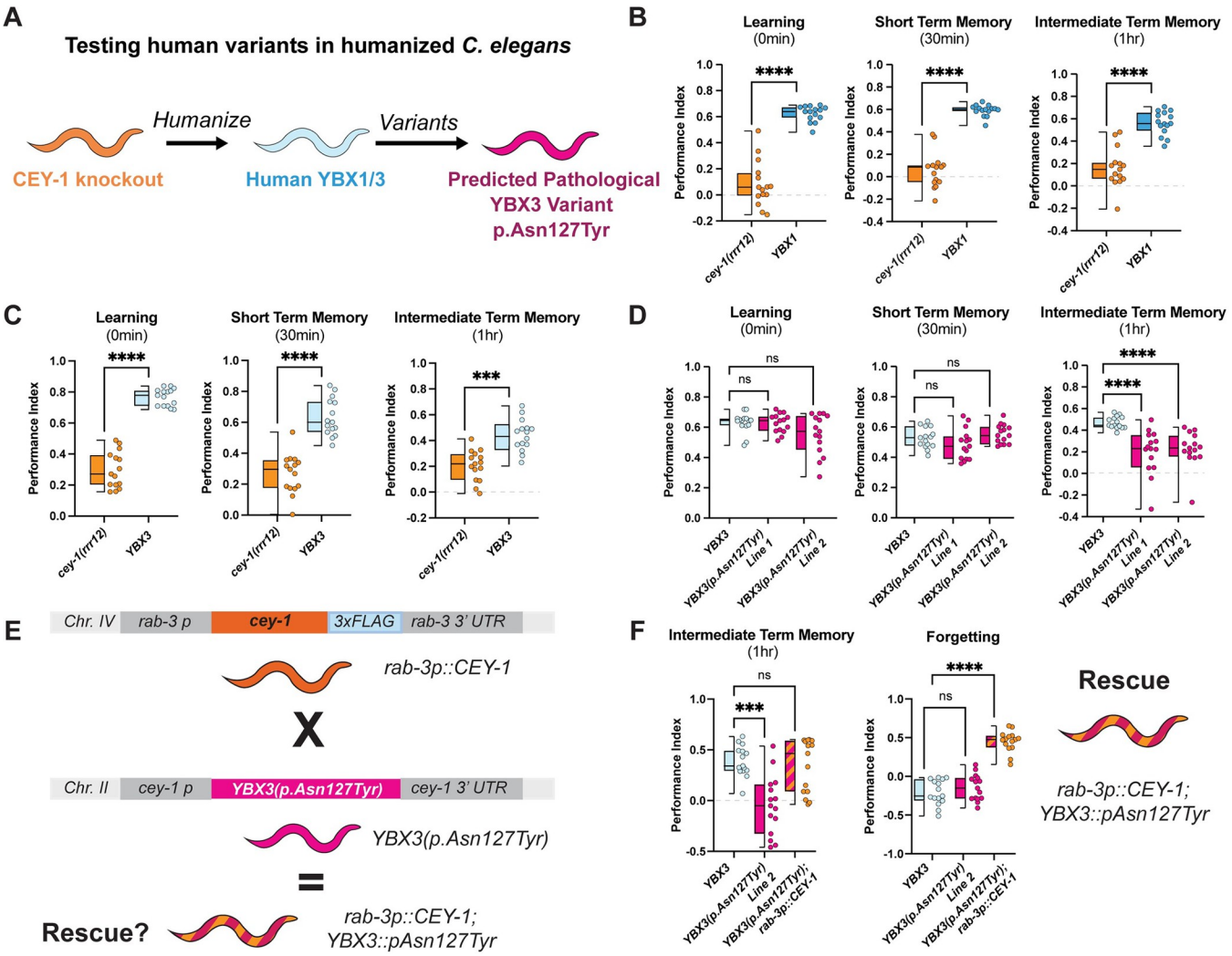


**Fig 5. Human *YBX1* and *YBX3* functionally replace *cey-1* in memory *in vivo* and insertion of a rare SNV into *YBX3* disrupts ITM.** (**A**) Diagram of workflow for humanizing *C. elegans* to express either human *YBX1* or human *YBX3*, then generating *YBX3* c.379A>T (p.Asn127Tyr). (**B**) Insertion of human *YBX1* into the endogenous *cey-1* locus rescues learning and memory deficits seen in *cey-1* knockout animals *(cey-1(rrr12))* back to wild-type levels (also see S12 Fig). (**C**) Insertion of human *YBX3* into the endogenous *cey-1* locus rescues learning and memory deficits seen in *cey-1* knockout animals *(cey-1(rrr12))* back to wild-type levels (also see S12 Fig). (**D**) Introduction of c.379A>T(p.Asn127Tyr) into the humanized *YBX3* locus causes ITM deficits. Box and whisker plot as in Fig 1. n = 15 per genotype. ****p<0.0001, ns, not significant (p>0.05). (**E**) Diagram of strategy to determine whether neuronal *cey-1* is sufficient to rescue and enhance memory in worms expressing *YBX3(p.Asn127Tyr)*. Worms that express a single copy of *cey-1* only in the nervous system *(rab-3p::cey-1::rab-3 3'UTR; cey-1(rrr12))* were crossed to those expressing patient variant *YBX3(p.Asn127Tyr)* and subsequently tested for phenotypic rescue in (F). (**F**) Neuronal expression of CEY-1 rescues intermediate term memory deficits observed in *YBX3(p.Asn127Tyr)* animals. n = 15, ***p<0.001, ****p<0.0001, ns, not significant (p>0.05).

https://doi.org/10.1371/journal.pgen.1011443.g005

*(p.Asn127Tyr);rab-3p::cey-1::rab-3 3'UTR* animals (Fig 5E) and found that introduction of a functional CEY-1 in the nervous system rescued the ITM deficits of *YBX3(p.Asn127Tyr)* animals (Fig 5F). Moreover, the *YBX3(p.Asn127Tyr)* variant did not appear to suppress the beneficial effects of an extra copy of wild-type CEY-1 on forgetting behaviors (Fig 5F). Together, these results suggest that *YBX3(p.Asn127Tyr)* is not dominant negative. As *YBX3* has a probability of loss-of-function intolerance (pLI) score of 0, this means the gene is tolerant of the functional loss of one copy of the gene. Therefore, our results suggest that *YBX3(pAsn127Tyr)* may confer a neomorphic effect.

## Discussion

### *C. elegans* as a discovery platform for novel associative memory regulators

We performed a targeted screen of 20 synaptically-enriched RBPs examining their roles in learning and memory and identified eight novel associative memory regulators, each regulating memory differently. While we focused on the CEY RBP family in this work, five other RBPs remain to be investigated. We found that *rbm-3.1* is required for STM, *rnp-5* is required for STM and ITM, *rpl-28* is required for STM and LTM, *rps-16* is required for STM, ITM, and LTM, and *eef-1B.2* suppresses STM. It is worth noting that the LTM-regulating RBPs were discovered using *egl-30(gf)* mutants with enhanced LTM that are extremely amenable to screening [51].Though previous work suggests that this memory requires the same molecules and neurons as LTM in wild-type animals [51], these results should be verified in wild-type animals prior to further study. *rbm-3.1*, ortholog of CIRP, is reported to mediate alcohol-induced spatial memory deficits in mice [121] but has never been associated with memory independently of alcohol use prior to this study. In addition, *eef-1B.2* and *rnp-5* are associated with human neurological disease. Pathogenic variants in EEF1B.2 cause autosomal recessive intellectual disability [122], while *rnp-5* ortholog RNPS1 is a risk factor for both intellectual disability and autism [123,124]. To our knowledge, neither *rps-16* nor *rpl-28* have been studied in the nervous system of any organism.

Here, we demonstrated novel roles for eight RBPs in memory using *C. elegans*. Our results suggest that these RBPs play a conserved role in memory that remains understudied, and future studies should combine worm behavior with human genetic data to examine these and other uncharacterized genes. Taken together, our study highlights the utility of *C. elegans* as a high-throughput screening tool for novel associative memory regulators, including those that regulate different, molecularly distinct forms of memory.

### Three of the four CEY RBPs are involved in memory

We identified three members of the CEY RBP family, orthologs of the mammalian YBX RBPs, as novel memory molecules. We found that each CEY RBP has its own distinct role in memory: *cey-1* regulates STM/ITM, *cey-2* regulates ITM, and *cey-3* regulates LTM. Of note, *cey-4* does not appear to be required for memory ability but is expressed throughout the adult nervous system [62,80,81], and therefore is likely involved in other neuronal functions. The unique role of each CEY in memory is not explained by their expression patterns, as *cey-1* and *cey-4* are both broadly expressed in the nervous system while *cey-2* and *cey-3* are found in very few neurons [62,80,81]. While evidence from the germline suggests the CEY RBPs are promiscuous in binding and are not affiliated with specific mRNA subsets [56], it is unclear whether there is more mRNA target specificity in the nervous system. Future studies examining how each CEY RBP regulates the translational landscape of neurons are warranted to determine the independent mechanisms by which the CEYs proteins regulate memory.

### CEY-1 is a novel neuronal memory-promoting RBP

Our study of CEY-1, the closest *C. elegans* ortholog to the mammalian YBX proteins, revealed that it acts in the nervous system to promote memory, as neuron-specific rescue of CEY-1 ameliorates behavioral defects cause by the loss of *cey-1* in multiple associative learning and memory paradigms, and an additional copy of CEY-1 only in the nervous system improves memory performance. Future investigations are needed to unveil the molecular mechanisms by which CEY-1 regulates memory, and whether or not it acts specifically at synapses, but based on known CEY/YBX biology and the fact that it may be generally required for learning

and memory, we hypothesize that CEY-1 controls transcription and/or translation of mRNAs involved in memory.

YBX1 is reported to bind to plasticity-associated mRNAs in an activity-dependent manner *in vitro* [68], and both CEY-1/YBX proteins regulate polysome formation and translation [56,70,71]. Furthermore, in non-neuronal tissues, YBX1 is reported to interact with known regulators of plasticity-dependent translation, specifically mTOR, AKT and translation initiation machinery [60,70,125]; therefore, it is likely that CEY-1/YBX is involved in these processes as well. Unlike other RBPs linked to plasticity-dependent translation, such as FMRP [126], YBX proteins are relatively non-specific with regards to target mRNAs [71,127]. It is unclear if a subset of molecules required for memory are regulated by YBX, or if it is involved in controlling broad machinery involved in plasticity and memory such as general protein synthesis. Future work will be necessary to determine the exact mechanisms by which CEY-1 promotes memory.

## YBX3 p.Asn127Tyr decreases intermediate term memory in a humanized *C. elegans* model

Given the lack of experimental evidence linking the mammalian YBX proteins to memory, we queried human variant datasets to explore potential associations between YBX dysfunction and neurological symptoms. We focused on *YBX1* and *YBX3* because they are expressed in the adult nervous system and found that several large CNVs involving either the *YBX1* or *YBX3* loci, as well as one rare missense YBX3 variant, are present in individuals with neurological symptoms including intellectual disability. However, the CNV analysis is limited by other disease-associated genes in the minimal overlap regions involving *YBX1* and *YBX3* and the SNV analysis is limited by the sample size and availability of de-identified clinical findings.

To assess the biological significance of rare, mono-allelic SNVs in either *YBX1* or *YBX3*, we conducted *in vivo* modeling of the variant with the highest pathogenicity scores. The YBX3 p.Asn127Tyr variant was identified in three individuals, two of whom exhibit neurological symptoms and one individual without neurological symptoms. The *YBX3* c.379A>T (p.Asn127Tyr) variant is located within the YBX3 CSD at a highly conserved site [76,77,127]. Introduction of the corresponding p.Asn56Tyr variant into the endogenous *cey-1* gene caused ITM deficits. We then decided to perform the same variant study in the context of human *YBX3*. Both *YBX1* and *YBX3* are able to functionally replace *cey-1*, as substitutions using either gene at the *cey-1* locus does not impair learning and memory. Introducing the *YBX3* c.379A>T (p.Asn127Tyr) variant into the humanized *C. elegans* line caused similar ITM deficits as the introduction of the variant into endogenous *cey-1*. Overall, these results suggest three key findings: one, that *cey-1* and *YBX3* are functionally conserved, two, that these data implicate both *YBX1* and *YBX3* in memory for the first time, and three, that *YBX3* c.379A>T (p.Asn127Tyr) may be of interest for future studies exploring the role of *YBX3* in human disease.

We believe that ITM deficits born from the introduction of the p.Asn127Tyr SNV may stem from dysregulation of mRNA translation by CEY-1/YBX3. The CSD, responsible for RNA binding, often lacks a highly specific affinity for a particular RNA motif [77,127]. As a result, proteins with CSDs are considered master regulators of the mRNA landscape. Though it is unclear how this mutation could affect CSD function and mRNA regulation based on the location of the amino acid, the p.Asn127Tyr mutation does add a bulky residue that could cause steric hindrance. A few possibilities for how this mutation might affect protein function, and therefore ability to properly regulate translation, include 1) disrupting interactions with other proteins, 2) affecting 3D conformation such that it impairs protein function, or 3)

altering protein stability due to misfolding. Though the mechanism is currently unknown, our data indicate that rare *YBX3* variants may be biologically significant and potentially affect neurologic function.

### Foundations for mammalian *in vivo* studies of YBX proteins in plasticity and neurological disease

Our finding of functional conservation between *C. elegans cey-1* and human *YBX1* and *YBX3* with regards to memory underscores the importance of future mammalian studies to determine the role of the *YBXs* in the nervous system. To date, studying the function of specific YBX proteins in mammalian models is challenging due to the potential for YBXs to genetically compensate for one another and the low survival rate of double knockouts [64]. Here, we report that either depleting CEY-1/YBX levels specifically in adulthood or introducing the rare *YBX3* c.379A>T (p.Asn127Tyr) variant detected in three human individuals disrupts memory. Each of these manipulations is less likely to be lethal or induce genetic compensation than complete loss during development. Future studies employing similar approaches in mammalian models will be extremely valuable. Moreover, future work will need to be considerate of loss of function mechanisms of variants. *YBX1* is predicted to be loss of function intolerant (pLI = 1, gnomAD v4.0), suggesting haploinsufficient variants may be deleterious. Conversely, *YBX3* is predicted to be loss of function tolerant (pLI = 0, gnomAD v4.0). Therefore, it is predicted that rare variants in *YBX3* that cause dysfunctions may be dominant-negative or result in gain-of-function. Interestingly, our behavioral data suggest that YBX3p.Asn127Tyr may be a neomorphic change manifesting as a reduction of function in our assays, as defects can be rescued with a wild-type copy of the protein. It is possible that other factors influence the penetrance of this mutation, which agrees with the finding that not all individuals with this variant exhibit neurological symptoms. Future identification of rare variants in the *YBX*s using comprehensive exome or genomic human datasets and modeling variants *in vivo* in mammals will enhance our understanding of mechanisms by which YBX dysfunction may play a role in human disease.

Taken together, our results uncover the CEY-1/YBX RBPs as novel associative memory regulators and potentially new contributors to rare neurological disease. Our current findings are limited to the functional testing of a single variant in *YBX3*. However, further examination of this protein class will provide new insights into the molecular mechanisms of memory and deepen our understanding of how disruption of RBPs contributes to disorders of the nervous system.

## Materials and methods

### *C. elegans* maintenance

All strains were maintained at 20˚C on 10cm plates made from standard nematode growth medium (NGM: 3g/L NaCl, 2.5g/L of Bacto-peptone, 17g/L Bacto-agar in milliQ water) or high nematode growth medium (HGM: 3g/L NaCl, 20g/L of Bacto-peptone, 30g/L Bacto-agar in milliQ water). After autoclaving and allowing molten agar to cool slightly, we added 1mL/L cholesterol (5mg/mL in ethanol), 1mL/L 1M $CaCl_2$, 1mL/L 1M $MgSO_4$, and 25mL/L 1M potassium phosphate buffer (pH 6.0) [128]. Experiments were performed using NGM plates seeded with OP50 *E. coli* as the food source for *ad libitum* feeding [128].

Hypochlorite population synchronization was performed by collecting eggs from gravid hermaphrodites via exposure to an alkaline-bleach solution (85mL water, 15mL sodium

hypochlorite, 5mL 5M NaOH), followed by repeated washing of collected eggs in 1mL of M9 buffer (6g/L $Na_2HPO_4$, 3g/L $KH_2PO_4$, 5g/L NaCl and 1mL/L 1M $MgSO_4$ in milliQ water [128]).

## Strains

Wild-type: (N2 Bristol)

Mutants: NM1380(*egl-30(js126))*, LC108(*uIs69[punc-119*::*sid-1; pmyo-2*::*mCherry])*, TU3401*(usIS69[myo-2p*::*mCherry + unc119p*::*sid-1]; sid-1(pk3321))*, RAF5(*cey-1(rrr12))*, VC1310*(cey-1(ok1805))*, GLW51*(cey-1(utx43[mNG*::*3xFLAG*::*cey-1]) II)*, OH13605*(otIs619 [unc-11(prom8)*::*2xNLS*::*TagRFP] X)* were obtained from the Caenorhabditis Genetics Center (University of Minnesota, Minneapolis, MN).

Nuclear GFP reporter for *cey-1* #1087*(cey-1p*::*PEST*::*GFPH2B*::*cey-1u; unc-119 was* described previously [56] and generously gifted by Rafal Ciosk.

Strains made in collaboration with InVivo Biosystems include: COP2655*(knuSi967[(rab-3p*::*CEY-1*::*3xFLAG*::*rab-3u*, *unc-119(+))] IV; unc-119(ed3) III)* and COP2656*(knuSi968[(rab-3p*::*CEY-1*::*3xFLAG*::*rab-3u*, *unc-119(+))] IV; unc-119(ed3) III)* are two lines with the same genotype, COP2689(*cey-1(knu1233 [N56Y]));* COP2721*((knu1251[YBX3]) II);* COP2763 ((*knu1275[YBX1]) II*); COP2774((*knu1286[p.N127Y]) II*) and COP2775((*knu1287[p.N127Y]*) II) are two lines with the same genotype.

The following strains were generated by crosses: RNA1*(egl-30(js126); uIs69[(pCFJ90)myo-2p*::*mCherry + unc-119p*::*sid-1])* was made by crossing NM1380*(egl-30(js126))* with LC108*(uIs69 [(pCFJ90)myo-2p*::*mCherry + unc-119p*::*sid-1])*. RNA20(*cey-1(utx43[mNG*::*3xFLAG*::*cey-1]) II; otIs619[unc-11(prom8)*::*2xNLS*::*TagRFP] X)* was made by crossing OH13605*(otIs619[unc-11 (prom8)*::*2xNLS*::*TagRFP] X)* with GLW51*(cey-1(utx43[mNG*::*3xFLAG*::*cey-1]) II)*. RNA26(*cey-1p*:: *PEST*::*GFPH2B*::*cey-1u; unc-119(+); otIs619[unc-11(prom8)*::*2xNLS*::*TagRFP] X)* was made by crossing OH13605*(otIs619[unc-11(prom8)*::*2xNLS*::*TagRFP] X)* with *cey-1* #1087*(cey-1p*::*PEST*::*GFPH2B*:: *cey-1u; unc-119(+))*. RNA40*(cey-1(rrr12); knuSi968[(rab-3p*::*CEY-1*::*3xFLAG*::*rab-3u*, *unc-119(+)] IV; unc-119(ed3) III)* was made by crossing RAF5(*cey-1(rrr12))* with COP2656*(knuSi968[(rab-3p*:: *CEY-1*::*3xFLAG*::*rab-3u*, *unc-119(+))] IV; unc-119(ed3) III)*. RNA44 (*cey-1(utx43[mNG*::*3xFLAG*:: *cey-1]) II; usIS69[myo-2p*::*mCherry + unc119p*::*sid-1]; sid-1(pk3321))* was made by crossing GLW51 *(cey-1(utx43[mNG*::*3xFLAG*::*cey-1]) II)* with TU3401*(usIS69[myo-2p*::*mCherry + unc119p*::*sid-1]; sid-1(pk3321))*. RNA47(*knu1286[p.N127Y]) II; knuSi968[(rab-3p*::*CEY-1*::*3xFLAG*::*rab-3u*, *unc-119 (+))] IV; unc-119(ed3) III*) was made by crossing COP2774((*knu1286[p.N127Y]) II*) with COP2656 *(knuSi968[(rab-3p*::*CEY-1*::*3xFLAG*::*rab-3u*, *unc-119(+))] IV; unc-119(ed3) III)*.

## RNAi treatment

For adult-only RNAi, worms that are neuronally sensitive to RNAi, RNA1*(egl-30(js126); uIs69 [(pCFJ90)myo-2p*::*mCherry + unc-119p*::*sid-1]))* and LC108 (*uIs69[(pCFJ90)myo-2p*::*mCherry + unc-119p*::*sid-1])*, or allow RNAi only in the nervous system, TU3401*(usIS69[myo-2p*:: *mCherry + unc119p*::*sid-1]; sid-1(pk3321))*, were synchronized by bleaching. Then, at L4, worms were transferred from plates seeded with OP50 to plates seeded with RNAi (*HT115 E. coli)* for *ad libitum* feeding and allowed to grow for two days. For all RNAi experiments, standard NGM molten agar was supplemented with 1mL/L IPTG (isopropyl β-d-1-thiogalactopyranoside) and 1mL/L 100mg/mL carbenicillin.

## Short-term and intermediate-term positive olfactory associative memory assays

Wild-type, mutant, or RNAi-treated worms were trained and tested for short- and intermediate-term memory changes as previously described [28]. Briefly, synchronized Day 2 adult

worms were washed off plates with M9 buffer. Worms were then allowed to settle by gravity and washed twice more with M9 buffer to remove any bacteria. After washing, the worms were starved for one hour in M9 buffer. For 1x food-butanone pairing, hereby called conditioning, starved worms were transferred to 10cm NGM conditioning plates seeded with OP50 *E. coli* bacteria and with a total of 16μL of 10% butanone (Sigma Aldrich) diluted in ethanol streaked on the lid in a '#' shape for one hour. After conditioning, the trained population of worms were tested for chemotaxis to 10% butanone and to an ethanol control using standard, previously described chemotaxis conditions [87]. Different stages of memory were tested by measuring chemotaxis of different subpopulations of worms at different timepoints at molecularly distinct stages of memory [29,30]. These stages are immediately after training (0min, learning) or after being transferred to 10cm NGM plates with fresh OP50 for 30 minutes (short-term associative memory), 1 hour (intermediate-term associative memory), or 2 hours (forgetting).

Chemotaxis indices for each timepoint were calculated as

Chemotaxis index = $(\#worms_{butanone}-\#worms_{ethanol})/(total\#worms)$.

Performance index is the change in the chemotaxis index after training relative to the untrained chemotaxis index, or

Performance index = $Chemotaxis\ index_{trained}$—$Chemotaxis\ index_{untrained}$

## Long-term positive olfactory associative memory assays

As previously published, *egl-30(js126)* animals form a long-term memory after just one round of training [51]. For LTM screening, we administered RNAi to adult, neuronally RNAi sensitive *egl-30(js126);punc119*::*sid-1* worms, performed S/ITM training (1 CS-US pairing), and measured learning immediately after training and long-term memory 16–20 hours post-training. Chemotaxis index and performance index were calculated in the same manner as short term and intermediate term associative memory assays.

## Aversive associative memory assays

As previously published [32], worms were tested for learning changes in response to aversive diacetyl training. Briefly, synchronized Day 2 adult worms were washed off plates with M9 buffer. Worms were then allowed to settle by gravity and washed twice more with M9 buffer to remove any bacteria. After washing, the worms were conditioned for one hour by starving on 10cm NGMs with no bacteria with 16uL of 100% diacetyl (Sigma Aldrich) streaked on the lid in a '#' shape. Immediately after conditioning, the trained population of worms were tested for chemotaxis to 1% diacetyl and to an ethanol control using standard, previously described chemotaxis conditions [87].

## Baseline chemosensation assays

Chemotaxis, or chemosensation experiments, were performed based on previously published assays [87]. In brief, assays were performed on unseeded 10cm NGMs. Two marks were made on the back of the plate on opposite sides of the plate, approximately 0.5cm from the edge. 1μL of sodium azide (Thermo Fisher) was placed on both spots and allowed to dry before adding 1μL of test odorant diluted in ethanol on one side and ethanol on the other. Odorants included 0.1% and 10% butanone (vol/vol), 0.1% nonanol (2-nonanone)(vol/vol), 1% isoamyl alcohol (vol/vol), 1% benzaldehyde (vol/vol), 10% pyrazine (weight/vol), and 1% diacetyl (vol/vol) (all from Sigma Aldrich). Worms were washed off their plates and subsequently washed three times with M9 buffer, then placed near the bottom center of the plate, equidistant between the

two marks, and allowed to chemotax for an hour. Chemotaxis indices for each timepoint were calculated as

Chemotaxis index = (#worms$_{odorant}$—#worms$_{ethanol}$)/(total#worms).

## % Origin motility assays

We measured motility as previously published [20] by finding the average percentage of worms remaining at the origin of the plate after a naïve (untrained) chemotaxis assay using an attractive concentration of butanone (0.1% vol/vol).

## Solid media motility assays

Worms were synchronized by hypochlorite treatment. 15–20 well-fed Day 2 adult worms on NGM plates seeded with OP50 *E. coli* were recorded for 60 second increments per group using a Nikon DS-Fi3 camera and NIS Elements Imaging Software. Videos were analyzed using wrMTrck software [129]. Data were thresholded such that only tracks of 15 seconds or longer were analyzed. Motility is reported as Average Speed (μm/sec) or Total distance in μm per track.

## Thrashing assays

Trashing assays were performed by first filling an unseeded 35mm NGM agar plate with 1mL of M9 buffer solution. Next, 10–15 well-fed Day 2 adult worms were transferred to an unseeded NGM agar plate to remove any bacteria stuck to the worms. All worms were then placed into the buffer for 1 minute to acclimate to the new environment. Thrashing behavior was recorded in 30 second increments per group of worms using a Nikon DS-Fi3 camera and NIS Elements Imaging Software. The number of thrashes per worm were quantified by manually counting the number of body bends; one body bend movement of the worm is defined by swinging its head and tail to the same side to form a C shape and then back to the initial position. This protocol was adapted from Nawa and Matsuoka 2012 [130].

## Confocal microscopy

Worms were paralyzed with fresh 4% levamisole diluted in M9 buffer and imaged for up to 30 minutes once put onto the slide to preserve protein dynamics. In all experiments, imaging of Day 2 adult worms was performed on a Nikon Ti2E inverted microscope system with a W1 spinning disk confocal unit at 100x magnification. For general CEY-1::mNG visualization, we used an excitation wavelength of 488nm for GFP and 561nm for RFP, used a pixel size of 0.11um/px, and z stacks with a z-step of 0.6μm. For quantification of CEY-1::mNG fluorescence after RNAi treatment, worms were imaged at 100X magnification, an excitation wavelength of 488nm, and z stacks with a z-step of 0.2 μm. Images were processed in Nikon NIS Elements software. The same settings for laser power and detector gain were used for all genotypes. For all images, red fluorescence was pseudo colored magenta and green fluorescence were pseudo colored cyan for colorblindness inclusivity. To quantify CEY-1::mNG fluorescence after RNAi knockdown, ImageJ [131] was used to quantify total fluorescence over a 100 μm square centered over the nerve ring after background subtraction.

## Variant identification and pathogenicity analysis

We received a deidentified dataset of human *YBX* gene variants identified through clinical exome and genome sequencing completed at Baylor Genetics [103] and removed any variants where symptomology listed could be explained by other genetic alterations found in the

individual's genome. Next, we removed any variants found in gnomAD v.2.1.1, even if only one case was reported [132], as these variants would not likely cause severe disease if found in the general population. We then selected variants for potential *in vivo* modeling based on the presence of neurological symptoms, such as seizures, microcephaly, autism, and intellectual disability. Variants of interest were then assessed using multiple pathogenicity metrics to determine the final variant for *in vivo* testing: specifically, M-CAP [110], SIFT [112], PolyPhen 2 [111], GERP [108], CADD [106,107], REVEL [109], and Phylop Vertebrate [113]. All metrics were found and visualized using the UCSC genome browser [133]. We selected the variant with the highest overall predicted pathogenicity across all score metrics as opposed to any specific numerical cutoffs. Pathogenicity of the p.Asn127Tyr variant on YBX3 protein function was predicted by using the YBX3 UniProt ID (P16989) as input for the following publicly available pipelines: AlphaMissense [119] and FunC-ESMs [120].

## Phylogenetic analysis

To analyze the evolutionary history and determine the similarity of RNA binding proteins between phyla, we used maximum likelihood (ML) analysis with the JTT matrix-based model [134]. We obtained protein sequences of the *C. elegans* CEY proteins as well as the human YBX proteins from UniProt [135] then used these sequences to generate a tree with the highest log likelihood score (-4517.57) using the Neighbor-Join and BioNJ algorithms to calculate pairwise distances from the JTT model. The tree was drawn to scale, with branch lengths measured in the number of substitutions per site and a 0.20 scale bar indicating the relative distance between nodes. All analyses were performed using MEGA X [74,136].

## Orthology analysis

Drosophila RNAi Screening Center Integration Ortholog Prediction Tool (DIOPT) is an online bioinformatics resource designed to facilitate the identification of orthologous genes across various species [75].

## RNA isolation, cDNA synthesis and qRT-PCR

Worms of a particular genotype were crushed in liquid nitrogen and added to Trizol (Thermo Fisher Scientific). RNA was isolated per manufacturer's instructions, followed by DNase treatment (Qiagen). cDNA was synthesized with an oligo dT primer and Superscript III reverse transcriptase enzyme (Thermo Fisher Scientific). cDNA was mixed with buffers, primers, SYBR green, and hot start Taq polymerase in a master mix prepared by a manufacturer (Thermo Fisher Scientific). Using a Quant Studio 7 Pro Dx Real-Time PCR System (Thermo Fisher Scientific), PCR reactions were run followed by a dissociation reaction to determine specificity of the amplified product. The amount of gene expression was quantified using the ΔΔCt method using *pmp-3* as a reference gene. Primer sets were as follows:

*cey-1* For: 5'-GGATCCAAGTATGCTGCCGA -3'
*cey-1* Rev: 5'- CCATCTGTGTCACGAGCAGT -3'
*pmp-3* For: 5'- AGTTCCGGTTGGATTGGTCC -3'
*pmp-3* Rev: 5'- CCAGCACGATAGAAGGCGAT-3'
*YBX3 WT* For: 5'- CCACCGTAACCCAACCTACC -3'
*YBX3 WT* Rev: 5'- CTTGGCCTCCTTTCCGTCTT -3'
*YBX3 p.Asn127Tyr* For: 5'- CGTCGTTACCGTCGTGGATA -3'
*YBX3 p.Asn127Tyr* Rev: 5'- TGGATACGGTTTGGGTGTGG -3'*YBX1* For: 5'- CTACCG TCGTTACCCACGTC -3'
*YBX1* Rev: 5'- ATCAGCTCCCTCCATGACCT -3'

### Statistical analysis

Statistical data is reported in the main text, figures, and tables as noted. Significance threshold of $p < 0.05$ was used. The symbols *, **, ***, and **** refer to $p < 0.05$, 0.01, 0.001, and 0.0001, respectively. For the comparison of performance indices between two behavior conditions (e.g. vector control vs *cey-1* RNAi), a Mann-Whitney test comparing ranks was used because it does not assume normality. For comparison of performance indices between three or more groups (e.g. wild-type vs two different *cey-1* loss-of-function mutants), one-way analysis of variances followed by Bonferroni post hoc tests for multiple comparisons were performed. For comparison of motility one-way analysis of variances followed by Games-Howell's multiple comparisons tests (due to larger Ns) were performed. Two-way ANOVAs were used for evaluating effects between genotype (Wild-type, *cey-1(rrr12)*, *YBX1*, *YBX3*) and timepoint (0hr, 0.5hr, 1hr, 2hr) on performance indices with a significant interaction between factors ($p<0.0001$) prompting Bonferroni post-hoc analyses to determine differences between individual groups. All experiments were repeated on separate days with separate populations to confirm reproducibility of results. Sample size n represents the number of chemotaxis assays performed for behavior, with each assay containing approximately 50–150 worms each.

### Statistical analysis software

All statistics and code were run in GraphPad Prism 10, using standard toolboxes.

## Supporting information

**S1 Fig. RNAi-based knockdown of RBPs does not have any detectable effect on learning ability.** Boxes signify 3+ RBPs in the same protein family or class (blue box include PUF RBPs, orange box includes CEY RBPs, grey box includes translation initiation machinery). Box and whisker plots are shown for the learning timepoints from the STM/ITM assays for each RBP screened. Box and whisker plot: the center line denotes the median value (50th percentile) while the box contains the 25th to 75th percentiles. Whiskers mark the 5th and 95th percentiles. ns, not significant ($p>0.05$).
(TIF)

**S2 Fig. RNAi-based knockdown of RBPs does not have any detectable effect on butanone sensing.** All RBPs in the screen are shown grouped by experiment. Bar represents mean. Whiskers mark the standard error of the mean. n = 10 per RNAi treatment. ns, not significant.
(TIF)

**S3 Fig. Summarized results of targeted screen of 20 RBPs.** All RBPs are shown where pink circles are decreased memory and blue circles are increased memory. The size of circle represents the p value from a combined $n \geq 5$–10 per RNAi treatment.
(TIF)

**S4 Fig. Results of targeted screen of 20 RBPs reveals both known and novel associative memory regulators.** All RBPs with significantly altered memory are shown divided by memory timepoint. Box and whisker plot: the center line denotes the median value (50th percentile) while the box contains the 25th to 75th percentiles. Whiskers mark the 5th and 95th percentiles. $n \geq 5$–10 per RNAi treatment. $^{*}p<0.05$,$^{**}p<0.01$, $^{***}p<0.001$, $^{****}p<0.0001$.
(TIF)

**S5 Fig. Images generated from publicly available VISTA (Visualizing the Spatial Transcriptome of the *C. elegans* Nervous System) [63]reveal differences in expression across each of the *cey* RBPs at L4.** While *cey-1* and *cey-4* have broad expression, *cey-2* is only located

in eight neurons at L4.
(TIF)

**S6 Fig. Data from multiple transcriptomic datasets as well as microscopy images reveal broad expression of CEY-1 in the nervous system of adult worms.** (A) Neuron-specific and/or single-cell RNA-seq data compiled from five different publications suggest *cey-1* mRNA is expressed in the adult nervous system [24, 35, 38, 43, 80, 137, 138]. (B) Diagram of microscopy images shown in (C). *C. elegans* head is labeled including the location of the pharynx and main neuronal ganglia/nerve rings. (C) A transcriptional *cey-1* reporter suggests the gene is broadly expressed in the neurons in the head at baseline conditions. Representative image of Day 2 adult worms with RFP-labeled neuronal nuclei (*unc-11(prom8)*::*2xNLS*::*TagRFP*)) pseudocolored magenta and a nuclear GFPH2B *cey-1* promoter fusion *(cey1p*::*GFPH2B*) pseudocolored cyan show colocalization.
(TIF)

**S7 Fig. Knockdown of *cey-1* specifically in the adult nervous system does not impair butanone sensing or motility.** (A) Naïve battery of both negative and positive odors reveals deficits in both nonanol and isoamyl alcohol chemotaxis, but not in benzaldehyde, pyrazine, or diacetyl chemotaxis at attractive concentrations. (B) Baseline chemosensation for butanone at neutral concentration of 10% is unaffected by neuron-specific knockdown of *cey-1*. n = 15 per RNAi treatment. (C) Baseline chemosensation for butanone at an attractive concentration of 0.1% is unaffected by neuron-specific knockdown of *cey-1*. n = 15 per RNAi treatment. (D) Motility, measured as proportion of worms at the origin of a chemotaxis plate, is unaffected by neuron-specific loss of *cey-1*. n = 15 per RNAi treatment. Box and whisker plot: the center line denotes the median value (50th percentile) while the box contains the 25th to 75th percentiles. Whiskers mark the 5th and 95th percentiles. $^{**}p<0.01$, $^{****}p<0.0001$. ns, not significant ($p>0.05$). (E) Representative images of adult-only, neuron-specific knockdown RNAi treatment (vector or *cey-1* RNAi) in neuronally RNAi-sensitized *mNG*::*CEY-1* animals. (F) Quantification of total fluorescent intensity. n = 26 for each RNAi condition. $^{*}p<0.05$.
(TIF)

**S8 Fig. *cey-1* loss-of-function mutants as well as worms with neuron-specific rescue of *cey-1* (*cey-1(rrr12)*; *rab-3p*::*CEY-1*) have no deficits in butanone sensing or motility, and neuron-specific rescue of *cey-1* restores learning and memory ability to wild-type levels.** (A) Naïve chemotaxis towards 10% butanone prior to behavioral conditioning does not significantly differ between wild-type animals, *cey-1(ok1805)*, and *cey-1(rrr12)* mutants. n = 15 per genotype. (B) Baseline chemosensation for butanone at an attractive concentration of 0.1% is unaffected by whole-body loss of *cey-1*. n = 15 per genotype. (C) Baseline chemosensation for butanone at an attractive concentration of 0.1% is unaffected by neuron-specific rescue of *cey-1*. n = 15 per genotype. (D) Motility, measured as proportion of worms at the origin of a chemotaxis plate, is unaffected by whole-body loss of *cey-1*. n = 15 per genotype. (E) Motility, measured as proportion of worms at the origin of a chemotaxis plate, is unaffected by neuron-specific rescue of *cey-1*. n = 15 per genotype. (F) Day 2 adult speed measured in μm/sec by Wrmtrck. n = 20–30 worms per genotype, Tracks were thresholded at 15 seconds duration, with multiple tracks per worm possible. ns, not significant. (G) Day 2 average track distance (in μm) traveled as measured by Wrmtrck. n = 20–30 worms per genotype, Tracks were thresholded at 15 seconds duration, with multiple tracks per worm possible. ns, not significant. Of note, for both F and G, wild-type controls for this figure are the same as S11 Fig because experiments were performed the same day each time; data was put into two separate graphs for organization. (H) Day 2 thrashing comparing number of body bends per 30 seconds of wild-

type, *cey-1(rrr12)* knockout worms, and nervous system specific rescue worms *(cey-1(rrr12); rab-3p*::*CEY-1)* shows that *cey-1* mutants do not have thrashing deficits, and indeed exhibit more body bends per minute. n = 50 for each genotype. (I) Associative memory curve comparing wild-type, *cey-1(rrr12)* knockout worms, and nervous system specific rescue worms *(cey-1 (rrr12);rab-3p*::*CEY-1)* shows that while knockouts have no associative learning or memory, neuron-specific rescue of *cey-1* allows for learning and memory equivalent to wild-type levels. Box and whisker plot: the center line denotes the median value (50th percentile) while the box contains the 25th to 75th percentiles. Whiskers mark the 5th and 95th percentiles. ns, not significant ($p>0.05$).
(TIF)

**S9 Fig. CNV gains and losses data for *YBX1* in DECIPHER [94].** (A) Percentages of individuals reported with gain or loss CNVs that include *YBX1*. (B) Percentages of mechanisms of inheritance of gain and loss CNVs that include *YBX1*. (C) Size of CNV gain and losses that include *YBX1*. (D) Predictive scores for *YBX1* from gnomAD v.2.11 [132] suggest that *YBX1* is intolerant to loss of function variants and is haploinsufficient. (E) Phenotypes of patients specifically with deletion/loss CNVs including *YBX1* include epicanthus, delayed speech and development, intellectual disability, and other neurological features.
(TIF)

**S10 Fig. CNV gains and losses data for *YBX3* in DECIPHER [94].** (A) Percentages of individuals reported with gain or loss CNVs that include *YBX3*. (B) Percentages of mechanisms of inheritance of gain and loss CNVs that include *YBX3*. (C) Size of CNV gain and losses that include *YBX3*. (D) Predictive scores for *YBX3* from gnomAD v.2.11 [132] suggest that *YBX3* is tolerant to loss of function variants and is haplosufficient, suggesting variants may instead be deleterious by being dominant negative or gain-of-function. (E) Phenotypes of patients specifically with deletion/loss CNVs including *YBX3*, primarily intellectual disability, low-set ears, micrognathia, and other neurological features.
(TIF)

**S11 Fig. Introduction of a point mutation from human individuals into *cey-1 (cey-1 (p. Asn56Tyr))* does not cause butanone sensing or motility defects.** (A) Baseline chemosensation for butanone at an attractive concentration of 0. 1% is unaffected by the p.Asn56Tyr variant in *cey-1*. n = 15 per genotype. (B) Motility, measured as proportion of worms at the origin of a chemotaxis plate, is unaffected by p.Asn56Tyr variant in *cey-1*. n = 15 per genotype. Box and whisker plot: the center line denotes the median value (50th percentile) while the box contains the 25th to 75th percentiles. Whiskers mark the 5th and 95th percentiles. ns, not significant ($p>0.05$). (C) qRT-PCR of *cey-1* mRNA levels in Day 2 adults shows that while *cey-1* knockouts *(cey-1(rrr12))* worms undergo nonsense mediated decay [56] resulting in reduced *cey-1* mRNA levels, introduction of the p.Asn56Tyr variant has no significant effect on *cey-1* expression. n = 6 per genotype. $^{**}p<0.01$. (D) Day 2 thrashing comparing number of body bends per 30 seconds of wild-type, neuron-specific CEY-1 overexpression *(cey-1(WT);rab-3p*::*CEY-1)*, and variant worms with p.Asn56Tyr in endogenous CEY-1 (*cey-1(p.Asn127Tyr)* shows that *cey-1* mutants do not have thrashing deficits, and indeed exhibit more body bends per minute. n = 50 for each genotype. Of note, wild-type controls for this figure are the same as S8 Fig because experiments were performed the same day each time; data was put into two separate graphs for organization. (E) Day 2 adult speed measured in μm/sec by Wrmtrck. n = 20–30 worms per genotype, Tracks were thresholded at 15 seconds duration, with multiple tracks per worm possible. ns, not significant. (F) Day 2 average track distance (in μm) traveled as measured by Wrmtrck. n = 20–30 worms per genotype, Tracks were thresholded at 15

seconds duration, with multiple tracks per worm possible. ns, not significant. Of note, for both E and F, wild-type controls for this figure are the same as S8 Fig because experiments were performed the same day each time; data was put into two separate graphs for organization.
(TIF)

**S12 Fig. Humanized lines expressing *YBX1* or *YBX3*, including those with a SNV in *YBX3*, have normal butanone sensing and motility.** (A) Associative memory curve comparing wild-type, *cey-1* knockouts, and humanized lines expressing either *YBX1* or *YBX3* at the endogenous *cey-1* locus. While worms expressing *YBX3* have normal memory performance, those expressing *YBX1* appear to have extended memory, as they have a strong association for butanone even two hours post-training. (B) Baseline chemosensation for butanone at an attractive concentration of 0.1% is normal in worms expressing *YBX1*. n = 15 per genotype. (C) Motility, measured as proportion of worms at the origin of a chemotaxis plate, is unaffected by *YBX1*. n = 15 per genotype. (D) Baseline chemosensation is normal in worms expressing *YBX3* at the *cey-1* locus. n = 15 per genotype. (E) Motility is unaffected by *YBX3*. n = 15 per genotype. (F) Baseline chemosensation is unaffected by expressing *YBX3(p.Asn127Tyr)* at the *cey-1* locus. n = 15 per genotype. (G) Motility is unaffected by *YBX3(p.Asn127Tyr)*. n = 15 per genotype. (H) qRT-PCR of *cey-1* and *YBX* mRNA levels in Day 2 adults shows that levels of *YBX1*, *YBX3*, and *YBX3(pAsn127Tyr)* are not significantly reduced compared to wild-type *cey-1* mRNA levels and therefore, introduction of the p.Asn127Tyr variant has no significant effect on expression. n = 5 per genotype. ns, not significant.
(TIF)

**S13 Fig. Location of the Asn127 residue based on Alphafold visualization of the human YBX3 protein.** (A) Forward-facing view of the protein with the β sheet that binds RNA facing the viewer. (B) Top-down view of the YBX3 protein depicts the location of the Asn127 residue.
(TIF)

**S1 Table. Detailed information for all individuals with CNV deletions in *YBX1* or *YBX3* included in Fig 4 and accompanying DECIPHER phenotypic data.**
(XLSX)

**S1 Data. Source Data For All Files and Figures.**
(XLSX)

## Acknowledgments

We thank the Ciosk lab for generously sharing the *cey-1* #1087 strain; the CGC for strains; Ben Jussila and In Vivo Biosystems for strains and helpful discussion; Peter Boag for helpful discussion; and members of the Arey lab, particularly Katie L Brandel and Catherine Stuart for their detailed feedback on the manuscript. We thank Drs. Jill Rosenfeld and Hongzheng Dai from Baylor Genetics for confirming the presence and relevance of the *YBX3 p.Asn127Tyr* variant. We thank Dr. Katka Cermakova from Baylor College of Medicine, and Dr. Amelie Stein from University of Copenhagen for discussion of potential effects of the p.Asn127Tyr variant on protein function. This study makes use of data generated by the DECIPHER community. A full list of centers who contributed to the generation of the data is available from https://deciphergenomics.org/about/stats and via email from contact@deciphergenomics.org. DECIPHER is hosted by EMBL-EBI.

## Author Contributions

**Conceptualization:** Ashley N. Hayden, Jill A. Rosenfeld, Rachel N. Arey.

**Formal analysis:** Hsiao-Tuan Chao, Jill A. Rosenfeld, Rachel N. Arey.

**Funding acquisition:** Rachel N. Arey.

**Investigation:** Ashley N. Hayden, Katie L. Brandel, Edward W. Pietryk, Paul R. Merlau, Priyadharshini Vijayakumar, Emily J. Leptich, Elizabeth S. Gaytan, Meredith I. Williams, Connie W. Ni, Rachel N. Arey.

**Methodology:** Ashley N. Hayden, Rachel N. Arey.

**Supervision:** Hsiao-Tuan Chao, Jill A. Rosenfeld, Rachel N. Arey.

**Validation:** Rachel N. Arey.

**Visualization:** Ashley N. Hayden, Rachel N. Arey.

**Writing – original draft:** Ashley N. Hayden, Rachel N. Arey.

**Writing – review & editing:** Ashley N. Hayden, Katie L. Brandel, Edward W. Pietryk, Elizabeth S. Gaytan, Connie W. Ni, Hsiao-Tuan Chao, Jill A. Rosenfeld, Rachel N. Arey.

## References

1. Costa-Mattioli M, Sossin WS, Klann E, Sonenberg N. Translational control of long-lasting synaptic plasticity and memory. Neuron. 2009; 61:10–26. https://doi.org/10.1016/j.neuron.2008.10.055 PMID: 19146809
2. Martin KC, Casadio A, Zhu H, Yaping E, Rose JC, Chen M, et al. Synapse-specific, long-term facilitation of aplysia sensory to motor synapses: a function for local protein synthesis in memory storage. Cell. 1997; 91:927–938. https://doi.org/10.1016/s0092-8674(00)80484-5
3. Hafner A-S, Donlin-Asp PG, Leitch B, Herzog E, Schuman EM. Local protein synthesis is a ubiquitous feature of neuronal pre- and postsynaptic compartments. Science. 2019:364. https://doi.org/10.1126/science.aau3644
4. Akins MR, Berk-Rauch HE, Fallon JR. Presynaptic translation: stepping out of the postsynaptic shadow. Front Neural Circuits. 2009; 3:17. https://doi.org/10.3389/neuro.04.017.2009 PMID: 19915727
5. Schieweck R, Ninkovic J, Kiebler MA. RNA-binding proteins balance brain function in health and disease. Physiol Rev. 2021; 101:1309–1370. https://doi.org/10.1152/physrev.00047.2019
6. Doxakis E. RNA binding proteins: a common denominator of neuronal function and dysfunction. Neurosci Bull. 2014; 30:610–626. https://doi.org/10.1007/s12264-014-1443-7 PMID: 24962082
7. Gebauer F, Schwarzl T, Valcárcel J, Hentze MW. RNA-binding proteins in human genetic disease. Nat Rev Genet. 2021; 22:185–198. https://doi.org/10.1038/s41576-020-00302-y
8. Prashad S, Gopal PP. RNA-binding proteins in neurological development and disease. RNA Biol. 2021; 18: 972–987. https://doi.org/10.1080/15476286.2020.1809186 PMID: 32865115
9. Lauriat TL, Shiue L, Haroutunian V, Verbitsky M, Ares M, Ospina L, et al. Developmental expression profile of quaking, a candidate gene for schizophrenia, and its target genes in human prefrontal cortex and hippocampus shows regional specificity. J Neurosci Res. 2008; 86:785–796. https://doi.org/10.1002/jnr.21534
10. Au PYB, Goedhart C, Ferguson M, Breckpot J, Devriendt K, Wierenga K, et al. Phenotypic spectrum of Au-Kline syndrome: a report of six new cases and review of the literature. Eur J Hum Genet. 2018; 26:1272–1281. https://doi.org/10.1038/s41431-018-0187-2 PMID: 29904177
11. Dingemans AJM, Truijen KMG, Kim J-H, Alaçam Z, Faivre L, Collins KM, et al. Establishing the phenotypic spectrum of ZTTK syndrome by analysis of 52 individuals with variants in SON. Eur J Hum Genet. 2022; 30:271–281. https://doi.org/10.1038/s41431-021-00960-4 PMID: 34521999
12. Quartier A, Poquet H, Gilbert-Dussardier B, Rossi M, Casteleyn A-S, Portes V, et al. Intragenic FMR1 disease-causing variants: a significant mutational mechanism leading to Fragile-X syndrome. Eur J Hum Genet. 2017; 25:423–431. https://doi.org/10.1038/ejhg.2016.204 PMID: 28176767
13. Gennarino VA, Palmer EE, McDonell LM, Wang L, Adamski CJ, Koire A, et al. A Mild PUM1 Mutation Is Associated with Adult-Onset Ataxia, whereas Haploinsufficiency Causes Developmental Delay and Seizures. Cell. 2018; 172:924–936.e11. https://doi.org/10.1016/j.cell.2018.02.006 PMID: 29474920

14. Hentze MW, Castello A, Schwarzl T, Preiss T. A brave new world of RNA-binding proteins. Nat Rev Mol Cell Biol. 2018; 19:327–341. https://doi.org/10.1038/nrm.2017.130

15. Olshansky SJ, Goldman DP, Zheng Y, Rowe JW. Aging in America in the twenty-first century: demographic forecasts from the MacArthur Foundation Research Network on an Aging Society. Milbank Q. 2009; 87:842–862. https://doi.org/10.1111/j.1468-0009.2009.00581.x PMID: 20021588

16. Kim KW, Tang NH, Piggott CA, Andrusiak MG, Park S, Zhu M, et al. Expanded genetic screening in Caenorhabditis elegans identifies new regulators and an inhibitory role for NAD+ in axon regeneration. eLife. 2018:7. https://doi.org/10.7554/eLife.39756 PMID: 30461420

17. Poole RJ, Bashllari E, Cochella L, Flowers EB, Hobert O. A Genome-Wide RNAi Screen for Factors Involved in Neuronal Specification in Caenorhabditis elegans. PLoS Genet. 2011; 7:e1002109. https://doi.org/10.1371/journal.pgen.1002109 PMID: 21698137

18. Doitsidou M, Flames N, Topalidou I, Abe N, Felton T, Remesal L, et al. A combinatorial regulatory signature controls terminal differentiation of the dopaminergic nervous system in C. elegans. Genes Dev. 2013; 27:1391–1405. https://doi.org/10.1101/gad.217224.113 PMID: 23788625

19. McDiarmid TA, Belmadani M, Liang J, Meili F, Mathews EA, Mullen GP, et al. Systematic phenomics analysis of autism-associated genes reveals parallel networks underlying reversible impairments in habituation. Proc Natl Acad Sci USA. 2020; 117:656–667. https://doi.org/10.1073/pnas.1912049116 PMID: 31754030

20. Lakhina V, Arey RN, Kaletsky R, Kauffman A, Stein G, Keyes W, et al. Genome-wide functional analysis of CREB/long-term memory-dependent transcription reveals distinct basal and memory gene expression programs. Neuron. 2015; 85: 330–345. https://doi.org/10.1016/j.neuron.2014.12.029 PMID: 25611510

21. Sohrabi S, Mor DE, Kaletsky R, Keyes W, Murphy CT. High-throughput behavioral screen in C. elegans reveals Parkinson's disease drug candidates. Commun Biol. 2021; 4: 203. https://doi.org/10.1038/s42003-021-01731-z PMID: 33589689

22. Vukojevic V, Gschwind L, Vogler C, Demougin P, de Quervain DJ-F, Papassotiropoulos A, et al. A role for α-adducin (ADD-1) in nematode and human memory. EMBO J. 2012; 31: 1453–1466. https://doi.org/10.1038/emboj.2012.14 PMID: 22307086

23. Fenyves BG, Arnold A, Gharat VG, Haab C, Tishinov K, Peter F, et al. Dual Role of an mps-2/KCNE-Dependent Pathway in Long-Term Memory and Age-Dependent Memory Decline. Curr Biol. 2021; 31: 527–539.e7. https://doi.org/10.1016/j.cub.2020.10.069

24. Yao V, Kaletsky R, Keyes W, Mor DE, Wong AK, Sohrabi S, et al. An integrative tissue-network approach to identify and test human disease genes. Nat Biotechnol. 2018. https://doi.org/10.1038/nbt.4246 PMID: 30346941

25. Sharifnia P, Jin Y. Regulatory roles of RNA binding proteins in the nervous system of C. elegans. Front Mol Neurosci. 2014; 7: 100. https://doi.org/10.3389/fnmol.2014.00100 PMID: 25628531

26. Kamath RS, Ahringer J. Genome-wide RNAi screening in Caenorhabditis elegans. Methods. 2003; 30: 313–321. https://doi.org/10.1016/s1046-2023(03)00050-1

27. Calixto A, Chelur D, Topalidou I, Chen X, Chalfie M. Enhanced neuronal RNAi in C. elegans using SID-1. Nat Methods. 2010; 7: 554–559. https://doi.org/10.1038/nmeth.1463 PMID: 20512143

28. Kauffman AL, Ashraf JM, Corces-Zimmerman MR, Landis JN, Murphy CT. Insulin signaling and dietary restriction differentially influence the decline of learning and memory with age. PLoS Biol. 2010; 8: e1000372. https://doi.org/10.1371/journal.pbio.1000372 PMID: 20502519

29. Stein GM, Murphy CT. C. elegans positive olfactory associative memory is a molecularly conserved behavioral paradigm. Neurobiol Learn Mem. 2014; 115: 86–94. https://doi.org/10.1016/j.nlm.2014.07.011 PMID: 25108196

30. Kauffman A, Parsons L, Stein G, Wills A, Kaletsky R, Murphy C. C. elegans positive butanone learning, short-term, and long-term associative memory assays. J Vis Exp. 2011. https://doi.org/10.3791/2490 PMID: 21445035

31. Rankin CH, Beck CD, Chiba CM. Caenorhabditis elegans: a new model system for the study of learning and memory. Behav Brain Res. 1990; 37: 89–92. https://doi.org/10.1016/0166-4328(90)90074-o

32. Stetak A, Hörndli F, Maricq AV, van den Heuvel S, Hajnal A. Neuron-specific regulation of associative learning and memory by MAGI-1 in C. elegans. PLoS ONE. 2009; 4: e6019. https://doi.org/10.1371/journal.pone.0006019 PMID: 19551147

33. Anantharaman V, Koonin EV, Aravind L. Comparative genomics and evolution of proteins involved in RNA metabolism. Nucleic Acids Res. 2002; 30: 1427–1464. https://doi.org/10.1093/nar/30.7.1427 PMID: 11917006

34. Matia-González AM, Laing EE, Gerber AP. Conserved mRNA-binding proteomes in eukaryotic organisms. Nat Struct Mol Biol. 2015; 22: 1027–1033. https://doi.org/10.1038/nsmb.3128 PMID: 26595419

35. Kaletsky R, Yao V, Williams A, Runnels AM, Tadych A, Zhou S, et al. Transcriptome analysis of adult Caenorhabditis elegans cells reveals tissue-specific gene and isoform expression. PLoS Genet. 2018; 14: e1007559. https://doi.org/10.1371/journal.pgen.1007559 PMID: 30096138

36. Holdorf AD, Higgins DP, Hart AC, Boag PR, Pazour GJ, Walhout AJM, et al. WormCat: An Online Tool for Annotation and Visualization of Caenorhabditis elegans Genome-Scale Data. Genetics. 2020; 214: 279–294. https://doi.org/10.1534/genetics.119.302919 PMID: 31810987

37. Kim W, Underwood RS, Greenwald I, Shaye DD. OrthoList 2: A New Comparative Genomic Analysis of Human and Caenorhabditis elegans Genes. Genetics. 2018; 210: 445–461. https://doi.org/10.1534/genetics.118.301307 PMID: 30120140

38. Arey RN, Kaletsky R, Murphy CT. Nervous system-wide profiling of presynaptic mRNAs reveals regulators of associative memory. Sci Rep. 2019; 9: 20314. https://doi.org/10.1038/s41598-019-56908-8 PMID: 31889133

39. Ostroff LE, Santini E, Sears R, Deane Z, Kanadia RN, LeDoux JE, et al. Axon TRAP reveals learning-associated alterations in cortical axonal mRNAs in the lateral amgydala. eLife. 2019; 8. https://doi.org/10.7554/eLife.51607 PMID: 31825308

40. Kaletsky R, Lakhina V, Arey R, Williams A, Landis J, Ashraf J, et al. The C. elegans adult neuronal IIS/FOXO transcriptome reveals adult phenotype regulators. Nature. 2016; 529: 92–96. https://doi.org/10.1038/nature16483 PMID: 26675724

41. Nijssen J, Aguila J, Hoogstraaten R, Kee N, Hedlund E. Axon-Seq Decodes the Motor Axon Transcriptome and Its Modulation in Response to ALS. Stem Cell Reports. 2018; 11: 1565–1578. https://doi.org/10.1016/j.stemcr.2018.11.005 PMID: 30540963

42. Cajigas IJ, Tushev G, Will TJ, tom Dieck S, Fuerst N, Schuman EM. The local transcriptome in the synaptic neuropil revealed by deep sequencing and high-resolution imaging. Neuron. 2012; 74: 453–466. https://doi.org/10.1016/j.neuron.2012.02.036 PMID: 22578497

43. Arey R, Kaletsky R, Murphy CT. Profiling of presynaptic mRNAs reveals a role for axonal PUMILIOs in associative memory formation. BioRxiv. 2019. https://doi.org/10.1101/733428

44. Freytag V, Probst S, Hadziselimovic N, Boglari C, Hauser Y, Peter F, et al. Genome-Wide Temporal Expression Profiling in Caenorhabditis elegans Identifies a Core Gene Set Related to Long-Term Memory. J Neurosci. 2017; 37: 6661–6672. https://doi.org/10.1523/JNEUROSCI.3298-16.2017 PMID: 28592692

45. Lau HL, Timbers TA, Mahmoud R, Rankin CH. Genetic dissection of memory for associative and non-associative learning in Caenorhabditis elegans. Genes Brain Behav. 2013; 12: 210–223. https://doi.org/10.1111/j.1601-183X.2012.00863.x

46. Timbers TA, Rankin CH. Tap withdrawal circuit interneurons require CREB for long-term habituation in Caenorhabditis elegans. Behav Neurosci. 2011; 125: 560–566. https://doi.org/10.1037/a0024370

47. Rose JK, Kaun KR, Chen SH, Rankin CH. GLR-1, a non-NMDA glutamate receptor homolog, is critical for long-term memory in Caenorhabditis elegans. J Neurosci. 2003; 23: 9595–9599. https://doi.org/10.1523/JNEUROSCI.23-29-09595.2003 PMID: 14573539

48. Jin X, Pokala N, Bargmann CI. Distinct circuits for the formation and retrieval of an imprinted olfactory memory. Cell. 2016; 164: 632–643. https://doi.org/10.1016/j.cell.2016.01.007 PMID: 26871629

49. Lim JP, Fehlauer H, Das A, Saro G, Glauser DA, Brunet A, et al. Loss of CaMKI Function Disrupts Salt Aversive Learning in C. elegans. J Neurosci. 2018; 38: 6114–6129. https://doi.org/10.1523/JNEUROSCI.1611-17.2018 PMID: 29875264

50. Liu H, Wu T, Canales XG, Wu M, Choi M-K, Duan F, et al. Forgetting generates a novel state that is reactivatable. Sci Adv. 2022; 8: eabi9071. https://doi.org/10.1126/sciadv.abi9071 PMID: 35148188

51. Arey RN, Stein GM, Kaletsky R, Kauffman A, Murphy CT. Activation of gαq signaling enhances memory consolidation and slows cognitive decline. Neuron. 2018; 98: 562–574.e5. https://doi.org/10.1016/j.neuron.2018.03.039 PMID: 29656871

52. Dubnau J, Chiang A-S, Grady L, Barditch J, Gossweiler S, McNeil J, et al. The staufen/pumilio pathway is involved in Drosophila long-term memory. Curr Biol. 2003; 13: 286–296. https://doi.org/10.1016/s0960-9822(03)00064-2

53. Dong H, Zhu M, Meng L, Ding Y, Yang D, Zhang S, et al. Pumilio2 regulates synaptic plasticity via translational repression of synaptic receptors in mice. Oncotarget. 2018; 9: 32134–32148. https://doi.org/10.18632/oncotarget.24345 PMID: 30181804

54. Costa-Mattioli M, Gobert D, Stern E, Gamache K, Colina R, Cuello C, et al. eIF2alpha phosphorylation bidirectionally regulates the switch from short- to long-term synaptic plasticity and memory. Cell. 2007; 129: 195–206. https://doi.org/10.1016/j.cell.2007.01.050 PMID: 17418795

55. Gindina S, Botsford B, Cowansage K, LeDoux J, Klann E, Hoeffer C, et al. Upregulation of eIF4E, but not other translation initiation factors, in dendritic spines during memory formation. J Comp Neurol. 2021; 529: 3112–3126. https://doi.org/10.1002/cne.25158 PMID: 33864263

56. Arnold A, Rahman MM, Lee MC, Muehlhaeusser S, Katic I, Gaidatzis D, et al. Functional characterization of C. elegans Y-box-binding proteins reveals tissue-specific functions and a critical role in the formation of polysomes. Nucleic Acids Res. 2014; 42: 13353–13369. https://doi.org/10.1093/nar/gku1077 PMID: 25378320

57. Calculli G, Lee HJ, Shen K, Pham U, Herholz M, Trifunovic A, et al. Systemic regulation of mitochondria by germline proteostasis prevents protein aggregation in the soma of C. elegans. Sci Adv. 2021; 7. https://doi.org/10.1126/sciadv.abg3012 PMID: 34172445

58. Budkina K, El Hage K, Clément M-J, Desforges B, Bouhss A, Joshi V, et al. YB-1 unwinds mRNA secondary structures in vitro and negatively regulates stress granule assembly in HeLa cells. Nucleic Acids Res. 2021; 49: 10061–10081. https://doi.org/10.1093/nar/gkab748 PMID: 34469566

59. Kwon E, Todorova K, Wang J, Horos R, Lee KK, Neel VA, et al. The RNA-binding protein YBX1 regulates epidermal progenitors at a posttranscriptional level. Nat Commun. 2018; 9: 1734. https://doi.org/10.1038/s41467-018-04092-0 PMID: 29712925

60. Wang J-Z, Zhu H, You P, Liu H, Wang W-K, Fan X, et al. Upregulated YB-1 protein promotes glioblastoma growth through a YB-1/CCT4/mLST8/mTOR pathway. J Clin Invest. 2022;132. https://doi.org/10.1172/JCI146536 PMID: 35239512

61. Mehta S, McKinney C, Algie M, Verma CS, Kannan S, Harfoot R, et al. Dephosphorylation of YB-1 is Required for Nuclear Localisation During G2 Phase of the Cell Cycle. Cancers (Basel). 2020; 12. https://doi.org/10.3390/cancers12020315 PMID: 32013098

62. Taylor SR, Santpere G, Reilly M, Glenwinkel L, Poff A, McWhirter R, et al. Expression profiling of the mature *C. elegans* nervous system by single-cell RNA-Sequencing. BioRxiv. 2019. https://doi.org/10.1101/737577

63. Liska D, Wolfe Z, Norris A. VISTA: Visualizing the Spatial Transcriptome of the C. elegans Nervous System. BioRxiv. 2023. https://doi.org/10.1101/2023.04.28.538711 PMID: 37163055

64. Evans MK, Matsui Y, Xu B, Willis C, Loome J, Milburn L, et al. Ybx1 fine-tunes PRC2 activities to control embryonic brain development. Nat Commun. 2020; 11: 4060. https://doi.org/10.1038/s41467-020-17878-y PMID: 32792512

65. Unkrüer B, Pekcec A, Fuest C, Wehmeyer A, Balda MS, Horn A, et al. Cellular localization of Y-box binding protein 1 in brain tissue of rats, macaques, and humans. BMC Neurosci. 2009; 10: 28. https://doi.org/10.1186/1471-2202-10-28 PMID: 19323802

66. Wang Q, Ding S-L, Li Y, Royall J, Feng D, Lesnar P, et al. The allen mouse brain common coordinate framework: A 3D reference atlas. Cell. 2020; 181: 936–953.e20. https://doi.org/10.1016/j.cell.2020.04.007 PMID: 32386544

67. Regev A, Teichmann SA, Lander ES, Amit I, Benoist C, Birney E, et al. The human cell atlas. eLife. 2017; 6. https://doi.org/10.7554/eLife.27041 PMID: 29206104

68. Tanaka T, Ohashi S, Funakoshi T, Kobayashi S. YB-1 binds to GluR2 mRNA and CaM1 mRNA in the brain and regulates their translational levels in an activity-dependent manner. Cell Mol Neurobiol. 2010; 30: 1089–1100. https://doi.org/10.1007/s10571-010-9541-9

69. Distler U, Schmeisser MJ, Pelosi A, Reim D, Kuharev J, Weiczner R, et al. In-depth protein profiling of the postsynaptic density from mouse hippocampus using data-independent acquisition proteomics. Proteomics. 2014; 14: 2607–2613. https://doi.org/10.1002/pmic.201300520

70. Nekrasov MP, Ivshina MP, Chernov KG, Kovrigina EA, Evdokimova VM, Thomas AAM, et al. The mRNA-binding protein YB-1 (p50) prevents association of the eukaryotic initiation factor eIF4G with mRNA and inhibits protein synthesis at the initiation stage. J Biol Chem. 2003; 278: 13936–13943. https://doi.org/10.1074/jbc.M209145200

71. Skabkin MA, Kiselyova OI, Chernov KG, Sorokin AV, Dubrovin EV, Yaminsky IV, et al. Structural organization of mRNA complexes with major core mRNP protein YB-1. Nucleic Acids Res. 2004; 32: 5621–5635. https://doi.org/10.1093/nar/gkh889 PMID: 15494450

72. Kretov DA. Role of Y-Box Binding Proteins in Ontogenesis. Biochemistry Mosc. 2022; 87: S71–S4. https://doi.org/10.1134/S0006297922140061

73. Fotovati A, Abu-Ali S, Wang P-S, Deleyrolle LP, Lee C, Triscott J, et al. YB-1 bridges neural stem cells and brain tumor-initiating cells via its roles in differentiation and cell growth. Cancer Res. 2011; 71: 5569–5578. https://doi.org/10.1158/0008-5472.CAN-10-2805

74. Kumar S, Stecher G, Li M, Knyaz C, Tamura K. MEGA X: Molecular evolutionary genetics analysis across computing platforms. Mol Biol Evol. 2018; 35: 1547–1549. https://doi.org/10.1093/molbev/msy096 PMID: 29722887

75. Hu Y, Flockhart I, Vinayagam A, Bergwitz C, Berger B, Perrimon N, et al. An integrative approach to ortholog prediction for disease-focused and other functional studies. BMC Bioinformatics. 2011; 12: 357. https://doi.org/10.1186/1471-2105-12-357 PMID: 21880147

76. Yang X-J, Zhu H, Mu S-R, Wei W-J, Yuan X, Wang M, et al. Crystal structure of a Y-box binding protein 1 (YB-1)-RNA complex reveals key features and residues interacting with RNA. J Biol Chem. 2019; 294: 10998–11010. https://doi.org/10.1074/jbc.RA119.007545 PMID: 31160337

77. Budkina KS, Zlobin NE, Kononova SV, Ovchinnikov LP, Babakov AV. Cold Shock Domain Proteins: Structure and Interaction with Nucleic Acids. Biochemistry Mosc. 2020; 85: S1–S19. https://doi.org/10.1134/S0006297920140011

78. Kretov DA, Curmi PA, Hamon L, Abrakhi S, Desforges B, Ovchinnikov LP, et al. mRNA and DNA selection via protein multimerization: YB-1 as a case study. Nucleic Acids Res. 2015; 43: 9457–9473. https://doi.org/10.1093/nar/gkv822 PMID: 26271991

79. Eliseeva IA, Sogorina EM, Smolin EA, Kulakovskiy IV, Lyabin DN. Diverse Regulation of YB-1 and YB-3 Abundance in Mammals. Biochemistry Mosc. 2022; 87: S48–S167. https://doi.org/10.1134/S000629792214005X

80. Taylor SR, Santpere G, Weinreb A, Barrett A, Reilly MB, Xu C, et al. Molecular topography of an entire nervous system. Cell. 2021; 184: 4329–4347.e23. https://doi.org/10.1016/j.cell.2021.06.023 PMID: 34237253

81. Hammarlund M, Hobert O, Miller DM, Sestan N. The cengen project: the complete gene expression map of an entire nervous system. Neuron. 2018; 99: 430–433. https://doi.org/10.1016/j.neuron.2018.07.042 PMID: 30092212

82. White JG, Southgate E, Thomson JN, Brenner S. The structure of the nervous system of the nematode Caenorhabditis elegans. Philos Trans R Soc Lond B Biol Sci. 1986; 314: 1–340. https://doi.org/10.1098/rstb.1986.0056

83. Chalfie M, Sulston J. Developmental genetics of the mechanosensory neurons of Caenorhabditis elegans. Dev Biol. 1981; 82: 358–370. https://doi.org/10.1016/0012-1606(81)90459-0

84. Gahlot S, Singh J. Caenorhabditis elegans neuronal RNAi does not render other tissues refractory to RNAi. Proc Natl Acad Sci USA. 2024; 121: e2401096121. https://doi.org/10.1073/pnas.2401096121 PMID: 38768358

85. Cook SJ, Jarrell TA, Brittin CA, Wang Y, Bloniarz AE, Yakovlev MA, et al. Whole-animal connectomes of both Caenorhabditis elegans sexes. Nature. 2019; 571: 63–71. https://doi.org/10.1038/s41586-019-1352-7 PMID: 31270481

86. Nishida Y, Sugi T, Nonomura M, Mori I. Identification of the AFD neuron as the site of action of the CREB protein in Caenorhabditis elegans thermotaxis. EMBO Rep. 2011; 12: 855–862. https://doi.org/10.1038/embor.2011.120 PMID: 21738224

87. Bargmann CI, Hartwieg E, Horvitz HR. Odorant-selective genes and neurons mediate olfaction in C. elegans. Cell. 1993; 74: 515–527. https://doi.org/10.1016/0092-8674(93)80053-h

88. Chou JH, Bargmann CI, Sengupta P. The Caenorhabditis elegans odr-2 gene encodes a novel Ly-6-related protein required for olfaction. Genetics. 2001; 157: 211–224. https://doi.org/10.1093/genetics/157.1.211 PMID: 11139503

89. Choi JI, Lee HK, Kim HS, Park SY, Lee TY, Yoon K-H, et al. Odor-dependent temporal dynamics in Caenorhabitis elegans adaptation and aversive learning behavior. PeerJ. 2018; 6: e4956. https://doi.org/10.7717/peerj.4956 PMID: 29910981

90. Yoshida K, Hirotsu T, Tagawa T, Oda S, Wakabayashi T, Iino Y, et al. Odour concentration-dependent olfactory preference change in C. elegans. Nat Commun. 2012; 3: 739. https://doi.org/10.1038/ncomms1750

91. Luo L, Gabel CV, Ha H-I, Zhang Y, Samuel ADT. Olfactory behavior of swimming C. elegans analyzed by measuring motile responses to temporal variations of odorants. J Neurophysiol. 2008; 99: 2617–2625. https://doi.org/10.1152/jn.00053.2008

92. Kunitomo H, Sato H, Iwata R, Satoh Y, Ohno H, Yamada K, et al. Concentration memory-dependent synaptic plasticity of a taste circuit regulates salt concentration chemotaxis in Caenorhabditis elegans. Nat Commun. 2013; 4: 2210. https://doi.org/10.1038/ncomms3210

93. Nussbacher JK, Tabet R, Yeo GW, Lagier-Tourenne C. Disruption of RNA metabolism in neurological diseases and emerging therapeutic interventions. Neuron. 2019; 102: 294–320. https://doi.org/10.1016/j.neuron.2019.03.014 PMID: 30998900

94. Firth HV, Richards SM, Bevan AP, Clayton S, Corpas M, Rajan D, et al. DECIPHER: Database of Chromosomal Imbalance and Phenotype in Humans Using Ensembl Resources. Am J Hum Genet. 2009; 84: 524–533. https://doi.org/10.1016/j.ajhg.2009.03.010 PMID: 19344873

95. Online Mendelian Inheritance in Man, O. MIM 616035. John Hopkins University; 2019 Jun.

96. Online Mendelian Inheritance in Man, O. MIM 138140. John Hopkins University; 2023 Dec.

97. Online Mendelian Inheritance in Man, O. MIM 600618. John Hopkins University; 2021 Jan.

98. Online Mendelian Inheritance in Man, O. MIM 603507. John Hopkins University; 2022 Dec.

99. Online Mendelian Inheritance in Man, O. MIM 607175. John Hopkins University; 2009 Dec.

100. Lefebvre S, Bürglen L, Reboullet S, Clermont O, Burlet P, Viollet L, et al. Identification and characterization of a spinal muscular atrophy-determining gene. Cell. 1995; 80: 155–165. https://doi.org/10.1016/0092-8674(95)90460-3

101. Wang X, You B, Yin F, Chen C, He H, Liu F, et al. A presumed missense variant in the U2AF2 gene causes exon skipping in neurodevelopmental diseases. J Hum Genet. 2023; 68: 375–382. https://doi.org/10.1038/s10038-023-01128-2

102. Molitor L, Bacher S, Burczyk S, Niessing D. The molecular function of PURA and its implications in neurological diseases. Front Genet. 2021; 12: 638217. https://doi.org/10.3389/fgene.2021.638217 PMID: 33777106

103. Yang Y, Muzny DM, Xia F, Niu Z, Person R, Ding Y, et al. Molecular findings among patients referred for clinical whole-exome sequencing. JAMA. 2014; 312: 1870–1879. https://doi.org/10.1001/jama.2014.14601 PMID: 25326635

104. Mani A. Pathogenicity of de novo rare variants: challenges and opportunities. Circ Cardiovasc Genet. 2017; 10. https://doi.org/10.1161/CIRCGENETICS.117.002013 PMID: 29237683

105. Järvelä I, Määttä T, Acharya A, Leppälä J, Jhangiani SN, Arvio M, et al. Exome sequencing reveals predominantly de novo variants in disorders with intellectual disability (ID) in the founder population of Finland. Hum Genet. 2021; 140: 1011–1029. https://doi.org/10.1007/s00439-021-02268-1 PMID: 33710394

106. Kircher M, Witten DM, Jain P, O'Roak BJ, Cooper GM, Shendure J. A general framework for estimating the relative pathogenicity of human genetic variants. Nat Genet. 2014; 46: 310–315. https://doi.org/10.1038/ng.2892 PMID: 24487276

107. Rentzsch P, Witten D, Cooper GM, Shendure J, Kircher M. CADD: predicting the deleteriousness of variants throughout the human genome. Nucleic Acids Res. 2019; 47: D886–D894. https://doi.org/10.1093/nar/gky1016 PMID: 30371827

108. Davydov EV, Goode DL, Sirota M, Cooper GM, Sidow A, Batzoglou S. Identifying a high fraction of the human genome to be under selective constraint using GERP++. PLoS Comput Biol. 2010; 6: e1001025. https://doi.org/10.1371/journal.pcbi.1001025 PMID: 21152010

109. Ioannidis NM, Rothstein JH, Pejaver V, Middha S, McDonnell SK, Baheti S, et al. REVEL: an ensemble method for predicting the pathogenicity of rare missense variants. Am J Hum Genet. 2016; 99: 877–885. https://doi.org/10.1016/j.ajhg.2016.08.016 PMID: 27666373

110. Jagadeesh KA, Wenger AM, Berger MJ, Guturu H, Stenson PD, Cooper DN, et al. M-CAP eliminates a majority of variants of uncertain significance in clinical exomes at high sensitivity. Nat Genet. 2016; 48: 1581–1586. https://doi.org/10.1038/ng.3703

111. Adzhubei IA, Schmidt S, Peshkin L, Ramensky VE, Gerasimova A, Bork P, et al. A method and server for predicting damaging missense mutations. Nat Methods. 2010; 7: 248–249. https://doi.org/10.1038/nmeth0410-248 PMID: 20354512

112. Ng PC, Henikoff S. SIFT: Predicting amino acid changes that affect protein function. Nucleic Acids Res. 2003; 31: 3812–3814. https://doi.org/10.1093/nar/gkg509 PMID: 12824425

113. Pollard KS, Hubisz MJ, Rosenbloom KR, Siepel A. Detection of nonneutral substitution rates on mammalian phylogenies. Genome Res. 2010; 20: 110–121. https://doi.org/10.1101/gr.097857.109 PMID: 19858363

114. Lins J, Brock TJ, Hopkins CE, Hart AC. Generation of a C. elegans tdp-1 null allele and humanized TARDBP containing human disease-variants. MicroPubl Biol. 2023; 2023. https://doi.org/10.17912/micropub.biology.000693 PMID: 37351305

115. Illiano P, Lanzo A, Leo D, Paglione M, Zampi G, Gainetdinov RR, et al. A Caenorhabditis elegans model to study dopamine transporter deficiency syndrome. Eur J Neurosci. 2017; 45: 207–214. https://doi.org/10.1111/ejn.13366

116. Zhu B, Mak JCH, Morris AP, Marson AG, Barclay JW, Sills GJ, et al. Functional analysis of epilepsy-associated variants in STXBP1/Munc18-1 using humanized Caenorhabditis elegans. Epilepsia. 2020; 61: 810–821. https://doi.org/10.1111/epi.16464 PMID: 32112430

117. McCormick K, Brock T, Wood M, Guo L, McBride K, Kim C, et al. A Gene Replacement Humanization Platform for Rapid Functional Testing of Clinical Variants in Epilepsy-associated *STXBP1*. BioRxiv. 2021. https://doi.org/10.1101/2021.08.13.453827

**118.** Varadi M, Bertoni D, Magana P, Paramval U, Pidruchna I, Radhakrishnan M, et al. AlphaFold Protein Structure Database in 2024: providing structure coverage for over 214 million protein sequences. Nucleic Acids Res. 2024; 52: D368–D375. https://doi.org/10.1093/nar/gkad1011 PMID: 37933859

**119.** Cheng J, Novati G, Pan J, Bycroft C, Žemgulytė A, Applebaum T, et al. Accurate proteome-wide missense variant effect prediction with AlphaMissense. Science. 2023; 381: eadg7492. https://doi.org/10.1126/science.adg7492

**120.** Cagiada M, Jonsson N, Lindorff-Larsen K. Decoding molecular mechanisms for loss of function variants in the human proteome. BioRxiv. 2024. https://doi.org/10.1101/2024.05.21.595203

**121.** Jacob A, Ma Y, Nasiri E, Ochani M, Carrion J, Peng S, et al. Extracellular cold inducible RNA-binding protein mediates binge alcohol-induced brain hypoactivity and impaired cognition in mice. Mol Med. 2019; 25: 24. https://doi.org/10.1186/s10020-019-0092-3 PMID: 31146675

**122.** Gong P, Liu J, Jiao X, Niu Y, Wang J, Wang X, et al. Novel biallelic loss of EEF1B2 function links to autosomal recessive intellectual disability. Hum Mutat. 2022; 43: 299–304. https://doi.org/10.1002/humu.24329

**123.** Nguyen LS, Kim H-G, Rosenfeld JA, Shen Y, Gusella JF, Lacassie Y, et al. Contribution of copy number variants involving nonsense-mediated mRNA decay pathway genes to neuro-developmental disorders. Hum Mol Genet. 2013; 22: 1816–1825. https://doi.org/10.1093/hmg/ddt035

**124.** Gonatopoulos-Pournatzis T, Wu M, Braunschweig U, Roth J, Han H, Best AJ, et al. Genome-wide CRISPR-Cas9 Interrogation of Splicing Networks Reveals a Mechanism for Recognition of Autism-Misregulated Neuronal Microexons. Mol Cell. 2018; 72: 510–524.e12. https://doi.org/10.1016/j.molcel.2018.10.008

**125.** Lyabin DN, Eliseeva IA, Ovchinnikov LP. YB-1 synthesis is regulated by mTOR signaling pathway. PLoS ONE. 2012; 7: e52527. https://doi.org/10.1371/journal.pone.0052527 PMID: 23285076

**126.** Darnell JC, Van Driesche SJ, Zhang C, Hung KYS, Mele A, Fraser CE, et al. FMRP stalls ribosomal translocation on mRNAs linked to synaptic function and autism. Cell. 2011; 146: 247–261. https://doi.org/10.1016/j.cell.2011.06.013 PMID: 21784246

**127.** Kleene KC. Y-box proteins combine versatile cold shock domains and arginine-rich motifs (ARMs) for pleiotropic functions in RNA biology. Biochem J. 2018; 475: 2769–2784. https://doi.org/10.1042/BCJ20170956

**128.** Brenner S. The genetics of Caenorhabditis elegans. Genetics. 1974; 77: 71–94.

**129.** Nussbaum-Krammer CI, Neto MF, Brielmann RM, Pedersen JS, Morimoto RI. Investigating the spreading and toxicity of prion-like proteins using the metazoan model organism C. elegans. J Vis Exp. 2015; 52321. https://doi.org/10.3791/52321 PMID: 25591151

**130.** Nawa M, Matsuoka M. The Method of the Body Bending Assay Using Caenorhabditis elegans. Bio Protoc. 2012; 2. https://doi.org/10.21769/BioProtoc.253

**131.** Schindelin J, Arganda-Carreras I, Frise E, Kaynig V, Longair M, Pietzsch T, et al. Fiji: an open-source platform for biological-image analysis. Nat Methods. 2012; 9: 676–682. https://doi.org/10.1038/nmeth.2019 PMID: 22743772

**132.** Chen S, Francioli LC, Goodrich JK, Collins RL, Kanai M, Wang Q, et al. A genome-wide mutational constraint map quantified from variation in 76,156 human genomes. BioRxiv. 2022. https://doi.org/10.1101/2022.03.20.485034

**133.** Kent WJ, Sugnet CW, Furey TS, Roskin KM, Pringle TH, Zahler AM, et al. The human genome browser at UCSC. Genome Res. 2002; 12: 996–1006. https://doi.org/10.1101/gr.229102 PMID: 12045153

**134.** Jones DT, Taylor WR, Thornton JM. The rapid generation of mutation data matrices from protein sequences. Comput Appl Biosci. 1992; 8: 275–282. https://doi.org/10.1093/bioinformatics/8.3.275

**135.** Consortium UniProt. Uniprot: the universal protein knowledgebase in 2023. Nucleic Acids Res. 2023; 51: D523–D531. https://doi.org/10.1093/nar/gkac1052 PMID: 36408920

**136.** Stecher G, Tamura K, Kumar S. Molecular Evolutionary Genetics Analysis (MEGA) for macOS. Mol Biol Evol. 2020; 37: 1237–1239. https://doi.org/10.1093/molbev/msz312 PMID: 31904846

**137.** Wang X, Jiang Q, Song Y, He Z, Zhang H, Song M, Zhang X, Dai Y, Karalay O, Dieterich C, et al. Ageing induces tissue-specific transcriptomic changes in Caenorhabditis elegans. EMBO J. 2022 41, e109633. https://doi.org/10.15252/embj.2021109633 PMID: 35253240

**138.** Ange J., Weng Y, Stevenson ME, Kaletsky R, Moore RS, Zhou S, and Murphy CT. Adult Single-nucleus Neuronal Transcriptomes of Insulin Signaling Mutants Reveal Regulators of Behavior and Learning. BioRxiv. 2024. https://doi.org/10.1101/2024.02.07.579364 PMID: 38370779